

Entanglement Entropy of Free Fermions in Timelike Slices

Bowei Liu,¹ Hao Chen,^{1,2} and Biao Lian¹

¹*Department of Physics, Princeton University, Princeton, New Jersey 08544, USA*

²*Department of Electrical and Computer Engineering,
Princeton University, Princeton, New Jersey 08544, USA*

(Dated: December 19, 2023)

We define the entanglement entropy of free fermion quantum states in an arbitrary spacetime slice of a discrete set of points, and particularly investigate timelike (causal) slices. For 1D lattice free fermions with an energy bandwidth E_0 , we calculate the time-direction entanglement entropy S_A in a time-direction slice of a set of times $t_n = n\tau$ ($1 \leq n \leq K$) spanning a time length t on the same site. For zero temperature ground states, we find that S_A shows volume law when $\tau \gg \tau_0 = 2\pi/E_0$; in contrast, $S_A \sim \frac{1}{3} \ln t$ when $\tau = \tau_0$, and $S_A \sim \frac{1}{6} \ln t$ when $\tau < \tau_0$, resembling the Calabrese-Cardy formula for one flavor of nonchiral and chiral fermion, respectively. For finite temperature thermal states, the mutual information also saturates when $\tau < \tau_0$. For non-eigenstates, volume law in t and signatures of the Lieb-Robinson bound velocity can be observed in S_A . For generic spacetime slices with one point per site, the zero temperature entanglement entropy shows a clear transition from area law to volume law when the slice varies from spacelike to timelike.

I. INTRODUCTION

The entanglement entropy of a subsystem in a bipartite system [1–4] characterizes the spatial entanglement information of quantum states [5–7]. For instance, the entanglement entropy of gapped (gapless) ground states satisfies the area law [8–11] (area law with a logarithmic factor [12–19]), while topological orders can be detected via correction to the area law known as the topological entanglement entropy [20, 21]. Moreover, the subsystem entanglement entropy of excited states can exhibit either area law or volume law, indicating (many-body) localization or quantum chaos, respectively [11, 22, 23].

The spatial subregion entanglement entropy, although related to thermodynamics in many aspects including the eigenstate thermalization hypothesis [24–26] and black holes [8, 9, 27–30], is a nonlocal quantity. Therefore, we ask if entanglement entropy of quantum states can be defined in a timelike slice, such as an observer’s worldline, which would be locally observable. For free fermion models, we show that the entanglement entropy of a quantum state can be explicitly defined for any spacetime slice consisting of a discrete set of points, which has not been discussed in previous studies of spacetime quantum entanglement [31–43]. It is also different from the temporal entanglement entropy for influence matrix [44–48] or similar generalizations in tensor networks [49, 50], which is defined for an effective time-direction “quantum state”, instead of for the physical quantum state (see Sec. V, and supplementary material (SM) [51] Sec. II).

We particularly investigate the entanglement entropy of one-dimensional (1D) free lattice fermions in an on-site time-direction slice of discrete times separated by τ (Fig. 1b). For lattice fermions with an energy spectrum of range E_0 , we find the time-direction entanglement entropy of thermal states is maximal and temperature independent when $\tau \gg \tau_0 = 2\pi/E_0$, while stabilizes to the Calabrese-Cardy formula of 1D chiral fermions [12–14] when $\tau < \tau_0$ at zero temperature, indicating the exis-

tence of a continuous time limit ($\tau \rightarrow 0$). The mutual information at finite temperature also stabilizes when $\tau < \tau_0$. For non-eigenstates, the time-direction entanglement entropy exhibits volume law and can probe the Lieb-Robinson bound velocity. Moreover, we show that the entanglement entropy exhibits a crossover of behaviors between spacelike and timelike slices.

This paper is organized as follows. In Sec. II we formulate the generic definition of spacetime slice entanglement entropy of free fermion lattice models, from both operator and path integral formalisms. Then for the example of 1D free fermions, we study the entanglement entropy in the time-direction slice in Sec. III, and in generic spacelike and timelike linear spacetime slices in Sec. IV. We then discuss possible future developments in Sec. V.

II. ENTANGLEMENT ENTROPY OF FREE FERMIONS IN AN ARBITRARY SPACETIME SLICE

Consider a system with a total Hilbert space h_{tot} . For an arbitrary spacetime slice A (Fig. 1a), if a sub-Hilbert space h_A can be identified for it, we can define its reduced density matrix ρ_A and entanglement entropy S_A as

$$\rho_A = \text{tr}_{h_{A^c}}(\rho_{\text{tot}}), \quad S_A = -\text{tr}(\rho_A \ln \rho_A), \quad (1)$$

where h_{A^c} is the complement of h_A ($h_{\text{tot}} = h_A \otimes h_{A^c}$). To do so, we impose the Heisenberg picture, such that quantum states are time-independent, while operators at spacetime point (\mathbf{r}, t) are defined by

$$O_{\mathbf{r},j}(t) = e^{iHt} O_{\mathbf{r},j} e^{-iHt}, \quad (2)$$

where H is the Hamiltonian. We then define h_A as the *minimal* sub-Hilbert space such that the correlations of any operators $O_{\mathbf{r}_n,j}(t_n)$ at spacetime points (\mathbf{r}_n, t_n) in

slice A are calculable from the reduced density matrix ρ_A in h_A , namely,

$$\langle \prod_{\alpha \in A} O_{\mathbf{r}_{n_\alpha}, j_\alpha}(t_{n_\alpha}) \rangle = \text{tr} \left[\rho_A \prod_{\alpha \in A} O_{\mathbf{r}_{n_\alpha}, j_\alpha}(t_{n_\alpha}) \right]. \quad (3)$$

Such a sub-Hilbert space is generically difficult to identify, but as we shall show, it can be identified straightforwardly for free fermion models.

A. Definition in the Heisenberg picture

We now show how sub-Hilbert space h_A can be identified for free fermion models. Consider a lattice model (in any dimension) with a free fermion Hamiltonian of the fermion bilinear form

$$H = \sum_{i,j} c_{\mathbf{r}_i}^\dagger h_{ij} c_{\mathbf{r}_j}. \quad (4)$$

Assume each site \mathbf{r}_m has one fermion degree of freedom with annihilation operator $c_{\mathbf{r}_m}$ and creation operator $c_{\mathbf{r}_m}^\dagger$ at time $t = 0$, with anti-commutators $\{c_{\mathbf{r}_m}, c_{\mathbf{r}_n}^\dagger\} = \delta_{mn}$. In an arbitrary slice A with K discrete spacetime points (\mathbf{r}_n, t_n) , each annihilation operator $c_{\mathbf{r}_n}(t_n) = e^{iHt_n} c_{\mathbf{r}_n} e^{-iHt_n}$ at point (\mathbf{r}_n, t_n) is the linear combination of $c_{\mathbf{r}_m}$ at time $t = 0$. Accordingly, the anti-commutations between $c_{\mathbf{r}_n}(t_n)$ and $c_{\mathbf{r}_m}^\dagger(t_m)$ are not delta functions, but are still numbers:

$$\{c_{\mathbf{r}_m}(t_m), c_{\mathbf{r}_n}^\dagger(t_n)\} = B_{mn}, \quad (m, n \in A). \quad (5)$$

B_{mn} gives a $K \times K$ non-negative Hermitian commutation matrix B for the K points in slice A . By rewriting $B = Q_1 \Lambda Q_1^\dagger$ with Λ diagonal and Q_1 unitary, we can define a matrix $M = Q_2 \Lambda^{-1/2} Q_1^\dagger$ where Q_2 can be an arbitrary unitary matrix, such that M satisfies $M^\dagger M = B^{-1}$. Particularly, by QL decomposition, we choose Q_2 such that M is a lower triangular matrix for later purposes of path integral formalism. We can then write down an orthonormal fermion basis:

$$d_m = \sum_{n \in A} M_{mn} c_{\mathbf{r}_n}(t_n), \quad (6)$$

and their Hermitian conjugates d_m^\dagger ($1 \leq m \leq K$). It is straightforward to see [51] that they satisfy

$$\{d_m, d_n^\dagger\} = \delta_{mn}, \quad (7)$$

and thus form an orthonormal fermion basis. h_A is then the Hilbert space of the K fermion degrees of freedom d_m , which has a dimension $\dim[h_A] = 2^K$. Any correlations among $c_{\mathbf{r}_n}(t_n)$ and $c_{\mathbf{r}_m}^\dagger(t_m)$ are completely determined within h_A . We note that our method for identifying sub-Hilbert space h_A here is similar to the bulk Hilbert space reconstruction most recently studied in Ref. [43].

As an illustrative example, consider a lattice of 3 sites with corresponding fermion annihilation operators

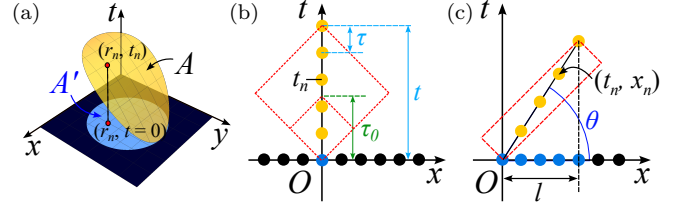


FIG. 1. (a) An arbitrary spacetime slice A (yellow) with discrete spacetime points (\mathbf{r}_n, t_n) at lattice sites \mathbf{r}_n and times t_n . In a 1D lattice fermion model, (b) shows a time-direction slice (yellow) of length t containing K points at times t_n ($1 \leq n \leq K$) on the same site $m = 0$; (c) shows a linear slice (yellow) containing points at $t_n = v_{\max}^{-1} x_n \tan(\theta)$ on the n -th site ($0 \leq n \leq \ell - 1$), with v_{\max} defined in Eq. (33).

c_1, c_2, c_3 , respectively, and assume spacetime slice A contains two spacetime points: $(x_1, t_1) = (x_1, 0)$ and (x_2, t_2) , with $t_1 = 0$ and $t_2 \neq 0$. Assume the free Hamiltonian H and time t_2 are such that, the fermion operators at these two points are

$$c_1(t_1) = c_1, \quad c_2(t_2) = \frac{1}{\sqrt{3}}(c_1 + c_2 + c_3). \quad (8)$$

Obviously, the above two fermion operators are not orthogonal, with their anti-commutation relation given by

$$\{c_m(t_m), c_n^\dagger(t_n)\} = B_{mn}, \quad B = \begin{pmatrix} 1 & \frac{1}{\sqrt{3}} \\ \frac{1}{\sqrt{3}} & 1 \end{pmatrix}. \quad (9)$$

To find the Hilbert space spanned by the two fermion operators $c_1(t_1)$ and $c_2(t_2)$, namely the sub-Hilbert space h_A of slice A , we need to find an orthonormal basis from linear superposition of $c_1(t_1)$ and $c_2(t_2)$, one choice of which is

$$\begin{aligned} d_1 &= c_1 = c_1(t_1), \\ d_2 &= \frac{1}{\sqrt{2}}(c_2 + c_3) = -\frac{1}{\sqrt{2}}c_1(t_1) + \sqrt{\frac{3}{2}}c_2(t_2), \end{aligned} \quad (10)$$

or in matrix form,

$$d_m = \sum_n M_{mn} c_n(t_n), \quad M = \begin{pmatrix} 1 & 0 \\ -\frac{1}{\sqrt{2}} & \sqrt{\frac{3}{2}} \end{pmatrix}. \quad (11)$$

This is the M matrix in Eq. (6), which satisfies

$$M^\dagger M = B^{-1}, \quad \rightarrow \quad \{d_m, d_n^\dagger\} = \delta_{mn}. \quad (12)$$

The sub-Hilbert space h_A spanned by $c_1(t_1)$ and $c_2(t_2)$ is thus the direct product of the fermion Hilbert space of d_1 and d_2 , which has dimension $\dim[h_A] = 2^2 = 4$.

For pure Fock states or thermal mixed states (or generically Gaussian states) with density matrix ρ_{tot} in the full system (which are time-independent in the Heisenberg picture here), the Wick's theorem holds, and thus the entanglement entropy S_A can be calculated from the

$K \times K$ two-point correlation matrix D in the orthonormal fermion basis d_m [52], with matrix elements:

$$D_{mn} = \text{tr}(\rho_{\text{tot}} d_m^\dagger d_n) = (M^* C M^T)_{mn} , \quad (13)$$

where C is the two-point correlation matrix in the space-time basis with matrix elements

$$C_{mn} = \text{tr} [\rho_{\text{tot}} c_{\mathbf{r}_m}^\dagger(t_m) c_{\mathbf{r}_n}(t_n)] . \quad (14)$$

By Wick's theorem, the entanglement entropy S_A in sub-Hilbert space h_A of slice A is determined by the two-point correlation matrix D as [52]

$$S_A = -\text{tr} [D \ln D + (I - D) \ln(I - D)] , \quad (15)$$

where I is the identity matrix.

We note that the choice of d_m fermion basis is not unique, but is up to a further unitary transformation (namely, the unitary matrix Q_2 in defining the M matrix can be arbitrary). However, the choice of d_m fermion operators does not change the entanglement entropy S_A , which is invariant under fermion basis unitary transformations.

When ρ_{tot} is a mixed state, it is known that the entanglement entropy S_A of sub-Hilbert space h_A (Eq. (15)) is not a measure of the entanglement between h_A and h_{A^c} , but is only a von-Neumann entropy. Instead, the entanglement between sub-Hilbert space h_A of slice A and its complement h_{A^c} can be characterized by the mutual information:

$$\mathcal{I} = S_A + S_{A^c} - S_{\text{tot}} , \quad (16)$$

where $S_{A^c} = -\text{tr}(\rho_{A^c} \ln \rho_{A^c})$ is the entanglement entropy of subsystem A^c , and $S_{\text{tot}} = -\text{tr}(\rho_{\text{tot}} \ln \rho_{\text{tot}})$ is the entanglement entropy of the entire system. For a pure state ρ_{tot} , one has $S_{\text{tot}} = 0$ and $\mathcal{I} = 2S_A$.

B. Path integral formalism

To provide an understanding of the above definition of entanglement entropy from a spacetime local perspective, in this subsection we rewrite it in terms of coherent state path integral formalism.

Conventionally, for a constant time t slice covering the full space, the coherent state basis for path integral is given by

$$|\eta(t)\rangle = \prod_j [1 - \eta_{\mathbf{r}_j}(t) c_{\mathbf{r}_j}^\dagger(t)] |0\rangle \quad (17)$$

where $\eta_{\mathbf{r}_j}(t)$ are anti-commuting Grassmann numbers (which also anti-commutes with fermion operators), and $\boldsymbol{\eta}(t) = (\eta_{\mathbf{r}_1}(t), \eta_{\mathbf{r}_2}(t), \dots)^T$ is the vector formed by all $\eta_{\mathbf{r}_j}(t)$. They give the values of the local fermion field $c_{\mathbf{r}_j}(t)$ at spacetime coordinate (\mathbf{r}_j, t) , namely:

$$c_{\mathbf{r}_j}(t) |\boldsymbol{\eta}(t)\rangle = \eta_{\mathbf{r}_j}(t) |\boldsymbol{\eta}(t)\rangle . \quad (18)$$

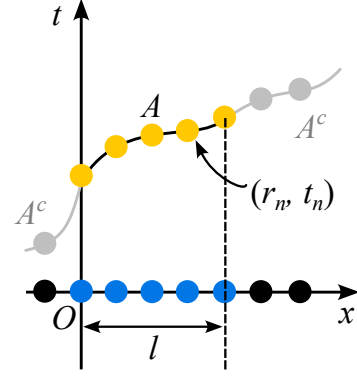


FIG. 2. Non-constant time slice A is part of a hypersurface $S = A \cup A^c$ that covers the entire space of the system.

The coherent states also satisfy the completeness condition:

$$\int D\boldsymbol{\eta}(t) D\bar{\boldsymbol{\eta}}(t) |\boldsymbol{\eta}(t)\rangle \langle \boldsymbol{\eta}(t)| = 1 . \quad (19)$$

For a free fermion model with Hamiltonian as shown in Eq. (4), the conventional path integral between two states at t_I and t_F is done by inserting the coherent state basis of constant time slices

$$\begin{aligned} \langle \boldsymbol{\eta}_F(t_F) | e^{-iH(t_F - t_I)} | \boldsymbol{\eta}_I(t_I) \rangle &= \int_{\boldsymbol{\eta}(t_I) = \boldsymbol{\eta}_I}^{\boldsymbol{\eta}(t_F) = \boldsymbol{\eta}_F} D\boldsymbol{\eta} D\bar{\boldsymbol{\eta}} \\ &\times e^{i \int_{t_I}^{t_F} dt [i \sum_j \bar{\eta}_{\mathbf{r}_j}(t) \partial_t \eta_{\mathbf{r}_j}(t) - \sum_{jl} h_{jl} \bar{\eta}_{\mathbf{r}_j}(t) \eta_{\mathbf{r}_l}(t)]} . \end{aligned} \quad (20)$$

Now for a non-constant time slice A shown in Fig. 2, we explain how to rewrite the path integral beginning or ending on slice A , which would be useful for defining the reduced density matrix ρ_A for slice A .

Suppose slice A is part of a hypersurface $S = A \cup A^c$ that covers the entire space of the system, where A^c is the complement of A satisfying $A \cap A^c = \emptyset$, as shown in Fig. 2. We note that the choice of A^c is arbitrary, and the entire hypersurface do not need to be “space-like”. For a space with L sites, we assume hypersurface S contains L spacetime points (\mathbf{r}_j, t_j) with fermion operators $c_{\mathbf{r}_j}(t_j)$, $c_{\mathbf{r}_j}^\dagger(t_j)$ defined in the Heisenberg picture. For convenience, we assume slice A contains K spacetime points, and we sort the spacetime points (\mathbf{r}_j, t_j) such that the first K points ($1 \leq j \leq K$) are those in slice A .

Our goal is to define a coherent state basis on hypersurface S satisfying

$$c_{\mathbf{r}_j}(t_j) |\boldsymbol{\eta}_S\rangle = \eta_{\mathbf{r}_j}(t_j) |\boldsymbol{\eta}_S\rangle , \quad (21)$$

where $\eta_{\mathbf{r}_j}(t_j)$ are Grassmann numbers and is grouped into a vector $\boldsymbol{\eta}_S = (\eta_{\mathbf{r}_1}(t_1), \eta_{\mathbf{r}_2}(t_2), \dots)^T$. To do this, we follow the same prescription as in Sec. II A: we define the anticommutation matrix in hypersurface S to be

$$\{c_{\mathbf{r}_j}(t_j), c_{\mathbf{r}_l}^\dagger(t_l)\} = B_{jl}^S , \quad (j, l \in S) \quad (22)$$

where it is easy to see that B^S is a Hermitian matrix. After diagonalizing it into $B^S = Q_1^S \Lambda^S Q_1^{S\dagger}$ with Λ^S diagonal and Q_1^S unitary, we define $N^S = (\Lambda^S)^{-\frac{1}{2}} Q_1^{S\dagger}$. We can then find a QL decomposition $N^S = Q_2^S M^S$ where Q_2^S is unitary and

$$M^S = Q_2^{S\dagger} (\Lambda^S)^{-\frac{1}{2}} Q_1^{S\dagger} = \begin{pmatrix} M & 0 \\ M' & M_c \end{pmatrix} \quad (23)$$

is a lower triangular matrix. It is easy to see that $M^{S\dagger} M^S = (B^S)^{-1}$. We have written M^S here into a block form with M being a $K \times K$ matrix and M_c a $(L-K) \times (L-K)$ matrix. Accordingly, both M and M_c are lower triangular. Also, $(M^S)^{-1}$ will be lower triangular.

We then define a new fermion complete basis d_j via

$$d_j = \sum_{l \in S} M_{jl}^S c_{\mathbf{r}_l}(t_l), \rightarrow c_{\mathbf{r}_j}(t_j) = \sum_{l \in S} (M^S)_{jl}^{-1} d_l, \quad (24)$$

which satisfies

$$\{d_j, d_l^\dagger\} = \delta_{jl}. \quad (25)$$

Since (M^S) and $(M^S)^{-1}$ are both lower triangular, the first K fermion operators d_j are only linear combinations of the first K fermion operators $c_{\mathbf{r}_j}(t_j)$ in slice A , and vice versa, reducing to the definition of fermion basis within slice A in Eq. (6). In the new basis of Eq. (24) on hypersurface S , we can define coherent states

$$|\eta_S\rangle = \prod_{j \in S} \left[1 - \sum_k \eta_{\mathbf{r}_k}(t_k) M_{jk}^S d_j^\dagger \right] |0\rangle, \quad (26)$$

which satisfies the definition of coherent states in Eq. (21):

$$\begin{aligned} c_{\mathbf{r}_j}(t_j) |\eta_S\rangle &= \sum_{l \in S} (M^S)_{jl}^{-1} d_l |\eta_S\rangle \\ &= \sum_{l, k \in S} (M^S)_{jl}^{-1} M_{lk}^S \eta_{\mathbf{r}_k}(t_k) |\eta_S\rangle = \eta_{\mathbf{r}_j}(t_j) |\eta_S\rangle. \end{aligned} \quad (27)$$

For fixed hypersurface S , the completeness condition is still satisfied:

$$|\det(M^S)|^2 \int D\eta_S D\bar{\eta}_S |\eta_S\rangle \langle \eta_S| = 1, \quad (28)$$

with $|\det(M^S)|^2$ being the Jacobian, which is a constant factor that can be absorbed into the measure of path integral.

We then note that such a coherent state can be decomposed as a direct product

$$|\eta_S\rangle = |\eta_A\rangle \otimes |\eta_{A^c}\rangle, \quad (29)$$

where

$$|\eta_A\rangle = \prod_{j \in A} \left[1 - \sum_{k \in A} \eta_{\mathbf{r}_k}(t_k) M_{jk}^S d_j^\dagger \right] |0\rangle \quad (30)$$

only depends on the values of $\eta_{\mathbf{r}_j}(t_j)$ in subregion A , due to the lower triangular form of matrix M^S . The other part $|\eta_{A^c}\rangle$ will depend on the values of $\eta_{\mathbf{r}_j}(t_j)$ in both A and A^c though.

In Schrodinger picture, consider a state with the density matrix $\rho_{\text{tot}}(0)$ at $t = 0$. In terms of path integral, we then define the density matrix on hypersurface S in the coherent state basis $|\eta_S\rangle$ as

$$\begin{aligned} \langle \eta'_S | \rho_{\text{tot}}(S) | \eta_S \rangle &= \int D\eta D\bar{\eta} \\ &\times e^{i \int_0^S dt (i\bar{\eta}^T \partial_t \eta - \bar{\eta}^T h \eta)} \rho_{\text{tot}}(0) e^{i \int_S^0 dt (i\bar{\eta}^T \partial_t \eta - \bar{\eta}^T h \eta)} \end{aligned} \quad (31)$$

where initial and final states in the path integral are given by $\eta_I = \eta_S$ and $\eta_F = \eta'_S$.

The reduced density matrix ρ_A in slice A is then defined by integrating out $\eta_{A^c} = \eta'_{A^c}$ in the path integral while fixing η_A and η'_A , which is equivalent to tracing over the Hilbert space generated by d_j with $j > K$. After this partial trace, ρ_A only depends on $\eta_{\mathbf{r}_j}(t_j) \in A$, which is equivalent to our formalism in Sec. II A. In this formalism, the path integral is spacetime local.

C. Model and definitions

We note that our definition of entanglement entropy in generic spacetime slice above holds for any free fermion models in any spacetime dimensions. For simplicity, hereafter, we investigate the spacetime slice entanglement entropy for the 1D tight-binding free fermion model with L sites and periodic boundary condition:

$$H = -u \sum_{m=0}^{L-1} \left(c_{m+1}^\dagger c_m + c_m^\dagger c_{m+1} \right), \quad (32)$$

where the hopping $u > 0$. The fermion energy at quasi-momentum k is $E(k) = -2u \cos(ka_0)$, where $a_0 = 1$ is the lattice constant. The energy bandwidth is $E_0 = 4u$. Accordingly, we define the characteristic time τ_0 and the maximal Fermi velocity (the Lieb-Robinson bound velocity [53]) v_{max} of the model as

$$\tau_0 = \frac{2\pi}{E_0}, \quad v_{\text{max}} = \max \left| \frac{dE(k)}{dk} \right| = 2ua_0. \quad (33)$$

Hereafter we set $u = \frac{1}{4}$. Besides, we denote the filling (average fermion number per site) as $\nu \in [0, 1]$.

III. TIME-DIRECTION SLICE

We now consider the case of slice A being a time-direction line segment of total time t on a fixed site $\mathbf{r}_n = 0$, containing K equally spaced points $(\mathbf{r}_n, t_n) = (0, (n-1)\tau)$, where $1 \leq n \leq K$, and $\tau = \frac{t}{K-1}$ is the spacing between adjacent times, as shown in Fig. 1b.

We first study the entanglement entropy S_A of thermal states ρ_{tot} at temperature T and filling ν in slice A , and then study that for non-eigenstates. We set $L \gg K$, for which S_A is independent of L .

A. Zero temperature

At temperature $T = 0$, ρ_{tot} is a pure state (ground state with a Fermi sea). For fixed total time t , as shown in Fig. 3a, within the range $K < t/\tau_0$, or equivalently $\tau > \tau_0$, S_A shows a triangular (trapezoid) shape curve with respect to K for filling $\nu = 0.5$ ($\nu \neq 0.5$); while in the range $K > t/\tau_0$, or $\tau < \tau_0$, S_A approaches a stabilized value. We further examine the total time t dependence of the stabilized value of S_A by fixing the time separation τ and changing the number of points $K = \frac{t}{\tau} + 1$. Interestingly, we find S_A is approximately linear in $\ln t$, where the slope $(\frac{\partial S_A}{\partial \ln K})_\tau \approx (\frac{\partial S_A}{\partial \ln t})_\tau$ is $\frac{1}{3}$ at $\tau = \tau_0$ [51], and quickly saturates to $\frac{1}{6}$ when $\tau < \tau_0$ (Fig. 3b). In addition, S_A shows an oscillation of period $\max(\frac{1}{\nu}, \frac{1}{1-\nu})$ with respect to K [51] at filling ν . These conclusions are insensitive to the energy dispersion [51].

The zero temperature S_A observed above can be understood in three regimes as follows. Assume $\Omega(E) \geq 0$ denotes the normalized density of states satisfying $\int \Omega(E) dE = 1$. For the time-direction slice A , the matrix in Eq. (5) reads

$$B_{mn} = \int e^{-iE(t_m - t_n)} \Omega(E) dE, \quad (34)$$

while the spacetime correlation matrix in Eq. (13) is

$$C_{mn} = \int \Omega(E) n_F(E) e^{iE(t_m - t_n)} dE \quad (35)$$

where $n_F(E)$ is the Fermi-Dirac distribution function at filling ν .

(i) When $\tau \gg \tau_0$, or $K \ll t/\tau_0$, one has

$$\begin{aligned} B_{mn} &\approx \delta_{mn} \int \Omega(E) dE = \delta_{mn}, \\ C_{mn} &\approx \delta_{mn} \int \Omega(E) n_F(E) dE = \nu \delta_{mn}, \end{aligned} \quad (36)$$

where the off-diagonal elements are suppressed by their fast oscillating integrands. This yields $D = M^* C M^T \approx \nu I$, and by Eq. (15) one has

$$S_A \approx K[-\nu \ln \nu - (1-\nu) \ln(1-\nu)]. \quad (\tau \gg \tau_0) \quad (37)$$

This fits well with the slope $(\frac{\partial S_A}{\partial K})_t$ at small K in Fig. 3a [51]. Moreover, if one approximates $\Omega(E)$ as uniform:

$$\Omega(E) = E_0^{-1} \Theta(E_0/2 - |E|), \quad (38)$$

where $\Theta(x) = 1$ ($= 0$) when $x > 0$ ($x < 0$), Eq. (37) becomes exact when $\nu = \frac{p}{q}$ ($p, q \in \mathbb{N}^+$ coprime) and

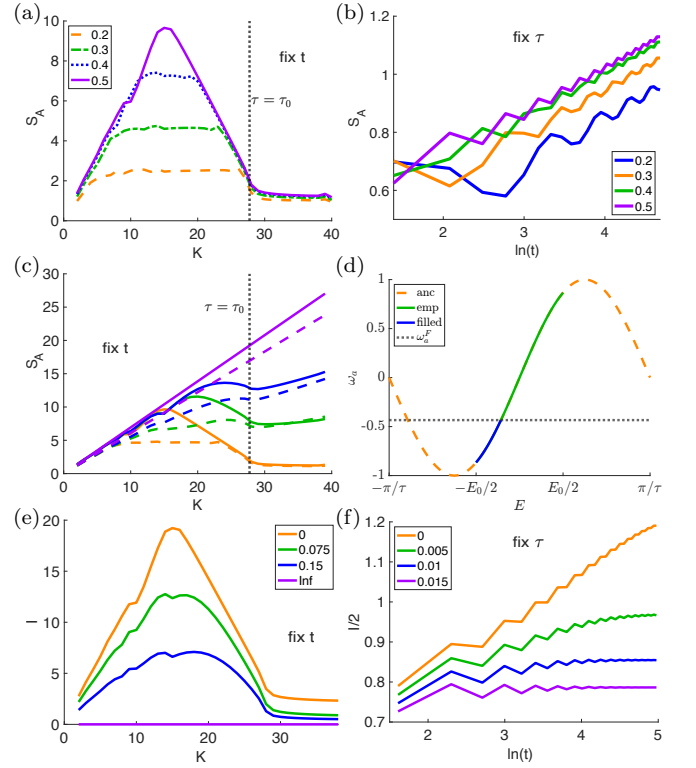


FIG. 3. (a)-(c) Entanglement entropy S_A of model Eq. (32) with $L = 500$ in time-direction slice of length t with K points separated by $\tau = t/(K-1)$, for (a) different filling ν given in the legend at temperature $T = 0$ and fixed $2\pi t/\tau_0 = 168$; (b) S_A versus $\ln t$ for different fillings ν (see legend) at $T = 0$ and fixed $\tau = \frac{2}{\pi}\tau_0$; (c) finite temperature S_A with fixed $2\pi t/\tau_0 = 168$, at fillings $\nu = 0.5$ (solid) and $\nu = 0.3$ (dashed). For each ν , the four curves from low to high have $T/E_0 = 0, 0.075, 0.15, \infty$, respectively. (d) The ancillary dispersion for explaining S_A when $\tau < \tau_0$ (“anc” for ancillary, “emp” for empty). (e)-(f) Mutual information \mathcal{I} with $L = 200$ at $\nu = 0.5$ and temperatures T/E_0 given in the legends while fixing (e) $2\pi t/\tau_0 = 168$ and (f) $\tau = \frac{5}{2\pi}\tau_0$, respectively.

$\tau = jq\tau_0$ ($j \in \mathbb{N}^+$). Eq. (37) also implies that $S_A \propto t = (K-1)\tau$ for fixed $\tau \gg \tau_0$. S_A in this limit is similar to the tensor network temporal entanglement entropy in [49, 50], although the definitions differ [51].

(ii) When $\tau = \tau_0$, or $K = \frac{t}{\tau_0} + 1$, taking the uniform $\Omega(E)$ approximation in Eq. (38), one has exactly

$$B_{mn} = E_0^{-1} \int_{-E_0/2}^{E_0/2} e^{-i(m-n)E\tau_0} dE = \delta_{mn}, \quad (39)$$

By Eq. (13), This gives

$$D_{mn} = C_{mn} = \frac{\tau_0}{2\pi} \int_{-\pi/\tau_0}^{\pi/\tau_0} n_F(E) e^{i(m-n)E\tau_0} dE, \quad (40)$$

Note that D_{mn} can be viewed as the *spatial* correlation matrix of a “lattice fermion model” with a “lattice constant” τ_0 , where E is the “quasi-momentum” in the “Brillouin zone” $[-\frac{\pi}{\tau_0}, \frac{\pi}{\tau_0}]$, and $n_F(E) = \Theta(E_F - E)$ for some

Fermi energy E_F . This is equivalent to a “zero temperature Fermi sea” state occupying “quasi-momentum” $-\frac{E_0}{2} \leq E \leq E_F$. By the Calabrese-Cardy formula [12–14], the zero-temperature entanglement entropy of 1D gapless states in a spatial subregion of length ℓ is $S_A = \frac{c_L + c_R}{6} \ln(\ell/\ell_c)$ with some constant ℓ_c , where c_L and c_R are the left and right central charges, respectively. Therefore, the zero-temperature time-direction entanglement entropy S_A at $\tau = \tau_0$ should resemble that of 1D gapless lattice fermion (nonchiral with $c_L = c_R = 1$) in a length t subregion:

$$S_A \approx \frac{1}{3} \ln\left(\frac{t}{t_c}\right) \approx \frac{1}{3} \ln\left(\frac{K\tau}{t_c}\right), \quad (\tau = \tau_0, T = 0) \quad (41)$$

where t_c is some constant.

(iii) When $\tau \ll \tau_0$, or $K \gg t/\tau_0$, if we enlarge the range of energy E from $[-\frac{E_0}{2}, \frac{E_0}{2}]$ to an ancillary range $[-\frac{\pi}{\tau}, \frac{\pi}{\tau}]$, we can think of E as the “quasi-momentum” in the Brillouin zone $[-\frac{\pi}{\tau}, \frac{\pi}{\tau}]$ of an “ancillary lattice fermion model” with lattice constant τ , which we assume has an ancillary dispersion $\omega_a(E)$ in Fig. 3d. Assume the ancilla model has a “Fermi level” $\omega_a^F = \omega_a(E_F)$. Meanwhile, the physical energy range $[-\frac{E_0}{2}, \frac{E_0}{2}]$ plays the role of a “quasi-momentum” cutoff near the right “Fermi surface” in Fig. 3d, keeping only the right-moving chiral fermions. As a result, the correlation matrix D resembles that of one right-moving chiral fermion mode. Thus, S_A stabilizes into the Calabrese-Cardy formula with $c_L = 0, c_R = 1$:

$$S_A \approx \frac{1}{6} \ln\left(\frac{t}{t'_c}\right) \approx \frac{1}{6} \ln\left(\frac{K\tau}{t'_c}\right). \quad (\tau \ll \tau_0, T = 0) \quad (42)$$

B. Finite temperature

At temperature $T > 0$, as shown in Fig. 3c, S_A for fixed total time t still shows a triangle or trapezoid like curve with respect to K when $K < t/\tau_0$ ($\tau > \tau_0$), and stabilizes into a linear relation when $K > t/\tau_0$ ($\tau < \tau_0$). The small K slope obeys Eq. (37) with a similar reasoning.

To characterize the entanglement between slice A and its complement, we calculate the mutual information \mathcal{I} in Eq. (16). For fixed total time t , \mathcal{I} at temperature $T > 0$ is shown in Fig. 3e, which shows stabilization at $K > t/\tau_0$ ($\tau < \tau_0$), similar to S_A at $T = 0$ (Fig. 3a). At $T = \infty$, one can show $\mathcal{I} \equiv 0$. For fixed $\tau < \tau_0$, we find \mathcal{I} increases at small t , and saturates as $t \gtrsim \beta = T^{-1}$, as shown in Fig. 3f.

C. Non-eigenstates

We now study S_A in time direction slice A of Fig. 1b at site $m = 0$ for pure non-eigenstates. We first consider state

$$|\psi_q\rangle = \prod_m c_{qm}^\dagger |0\rangle, \quad (43)$$

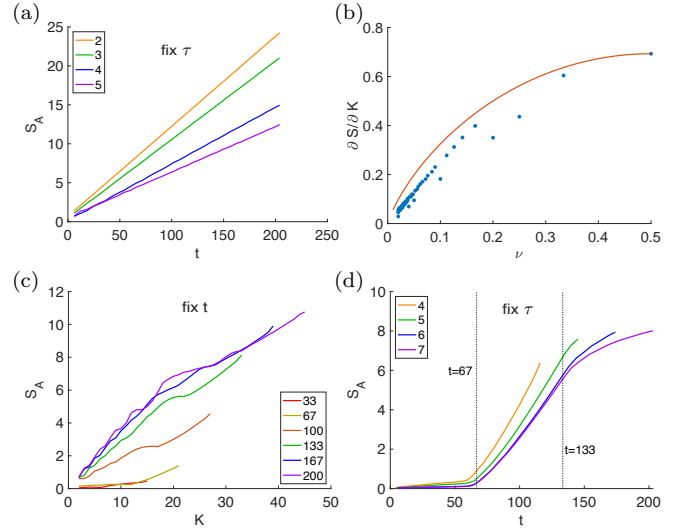


FIG. 4. Entanglement entropy S_A of time-direction slice of K points at site $m = 0$ for non-eigenstates (a)-(b) $|\psi_q\rangle = \prod_m c_{qm}^\dagger |0\rangle$ ($L = 500$) with fixed $2\pi\tau/\tau_0 = 6$, and (c)-(d) $|\psi\rangle = \prod_{-\frac{N_f}{3} < m < \frac{2N_f}{3}} c_m^\dagger |0\rangle$ ($L = 1000$) with $N_f = 100$. q is given in the legend of (a). In (b), the dots are the fitted $\left(\frac{\partial S_A}{\partial K}\right)_\tau$ and the red line is $-\nu \ln \nu - (1 - \nu) \ln(1 - \nu)$. (c) is calculated with fixed $2\pi t/\tau_0$ given in the legend, while (d) has fixed $2\pi\tau/\tau_0$ given in the legend.

with one occupied site per q sites ($q \in \mathbb{Z}$), which has filling $\nu \approx \frac{1}{q}$ (exact if q divides L). As shown in Fig. 4a, S_A with fixed spacing τ shows a volume law $S_A \propto t$, which has a slope $\left(\frac{\partial S_A}{\partial K}\right)_\tau$ upper bounded by $-\nu \ln \nu - (1 - \nu) \ln(1 - \nu)$, as shown in Fig. 4b. This is similar to that of thermal states ([51] Fig. S7), indicating the similarity between a partially filled pure state at finite energy density and a thermal state. Another state we calculate is

$$|\psi\rangle = \prod_{-\frac{N_f}{3} < m < \frac{2N_f}{3}} c_m^\dagger |0\rangle, \quad (44)$$

which has N_f consecutive occupied sites. As shown in Figs. 4c and 4d with $N_f = 100$, the behavior of S_A changes sharply as t reaches two times $t_L = \frac{N_f a_0}{3v_{\max}} \approx 67$ and $t_R = \frac{2N_f a_0}{3v_{\max}} \approx 133$, which correspond to the times for signals at two edges of the occupied interval to reach slice A . For $t < \min(t_L, t_R)$, S_A versus K with fixed t (Fig. 4c) or fixed τ (Fig. 4d) remains almost zero for $t < \min(t_L, t_R)$, resembling that of a fully occupied state. When $t > \min(t_L, t_R)$, Slice A sees the state as partially filled, and S_A starts to grow.

IV. LINEAR SPACETIME SLICES

We further investigate the entanglement entropy S_A in a linear spacetime slice at angle θ containing ℓ points at

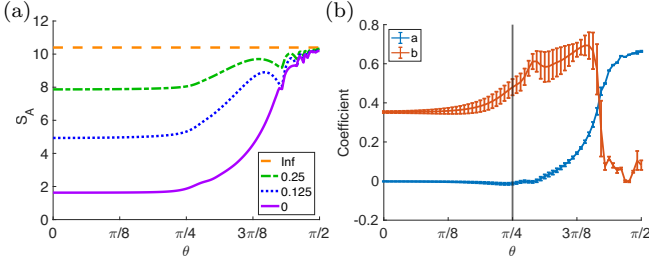


FIG. 5. (a) Entanglement entropy S_A as a function of θ with fixed $\ell = 15$ in the linear slice in Fig. 1c at $\nu = 0.5$ and T/E_0 given in the legend. (b) For the linear slice, we fit $S_A = a\ell + b\ln(\ell) + c$ to the zero temperature entanglement entropy at $1 \leq \ell \leq 20$. Then we plot a and b against θ . At $\theta = 0$, $a \approx 0$ and $b \approx 0.35$, which agrees with the theoretical prediction $S_A \approx \frac{1}{3} \ln(\ell/\ell_c)$. The value of a starts to increase significantly at around $\theta = 0.25\pi \sim 0.3\pi$, when the \ln term becomes sub-leading. When the linear term begins to saturate at $\theta \approx 0.4\pi$, b sharply drops to below 0.1. At $\theta = \frac{\pi}{2}$, $a \approx 0.66$ and $b \approx 0.08$, which also agrees with the theoretical prediction $S_A \approx \ln(2)\ell + c$.

$(x_n, t_n) = na_0(1, v_{\max}^{-1} \tan \theta)$, where $0 \leq n \leq \ell - 1$ (see Fig. 1c). Therefore, the slice is spacelike (non-causal) when $\theta < \frac{\pi}{4}$, and timelike (causal) when $\theta > \frac{\pi}{4}$. As shown in Fig. 5a, S_A for any temperature T thermal state stays nearly constant for $\theta < \frac{\pi}{4}$, while increases when $\theta > \frac{\pi}{4}$. This suggests an approximate “conformal symmetry” among all spacelike slices. We fit the zero temperature S_A by

$$S_A = a\ell + b\ln(\ell/\ell_c), \quad (45)$$

and the coefficients a and b as a function of θ are shown in Fig. 5b. We find $a \approx 0$ and $S_A \approx \frac{1}{3} \ln(\ell/\ell_c)$ for $\theta < \frac{\pi}{4}$, as expected from the Calabrese-Cardy formula [12–14]. For timelike slice with $\theta > \frac{\pi}{4}$, S_A shows a volume law with $a > 0$, and shows similarity to the time-direction slice case: as θ approaches $\frac{\pi}{2}$, the time separation $\tau = \frac{a_0}{v_{\max}} \tan \theta \gg \tau_0$, and S_A approaches Eq. (37) with $K = \ell$ points. To summarize, in this setup we find

$$S_A \approx \begin{cases} \frac{1}{3} \ln(\ell/\ell_c), & (\text{spacelike}), \\ a\ell, & (a > 0), \quad (\text{timelike}). \end{cases} \quad (46)$$

V. DISCUSSION

In this paper, we have defined a generalization of entanglement entropy in a generic spacetime slice for free fermion lattice models, as given by Eq. (15). We note that this spacetime entanglement entropy we defined easily applies to free bosons [52], which can similarly be calculated from two-point correlation functions.

For 1D free lattice fermion tight-binding model, we find the entanglement entropy in a time-direction slice

approaches Eq. (42), which holds when $\tau < \tau_0$. This indicates that the zero temperature time-direction entanglement entropy S_A of 1D free lattice fermions resembles the chiral Calabrese-Cardy formula $S_A = \frac{1}{6} \ln\left(\frac{t}{t_c}\right)$ in the continuous time limit $\tau \rightarrow 0$, given that the system size $L \gg K = \frac{t}{\tau} + 1$. A continuous time limit also exists for mutual information \mathcal{I} at finite temperature. When $K \geq L$, the Hilbert space h_A will saturates to h_{tot} (unless constrained by symmetries), leading to $S_A = S_{\text{tot}}$ [51].

Numerically, larger number of spacetime points K in slice A requires higher precision in the calculation of S_A . This can be simplified by defining a δ -cutoff of Hilbert space h_A . We approximate the $K \times K$ matrix B in Eq. (5) as $B \approx Q_\delta \Lambda_\delta Q_\delta^\dagger$, where Λ_δ is a $K_\delta \times K_\delta$ diagonal matrix with diagonals being the K_δ eigenvalues larger than δ (thus $K_\delta \leq K$), the eigenvectors of which are the columns of Q_δ . We can then define a matrix $M = \Lambda_\delta^{-1/2} Q_\delta^\dagger$ and an orthonormal basis of K_δ operators d_m by Eq. (6), which spans a sub-Hilbert space h_A^δ . We can calculate the zero temperature S_A and finite temperature \mathcal{I} for h_A^δ , which well approximate those for h_A when the cutoff δ is small enough [51].

An interesting question is the relation between our spacetime entanglement entropy and the temporal entanglement entropy of influence matrix [44–50], which differ in definitions and scaling behaviors (see [51] Sec. II for details). A key difference is as follows. Since $c_{r_m}(t_m), c_{r_m}(t_m)^\dagger$ at different spacetime points (r_m, t_m) in slice A do not form an orthogonal fermion basis, the local Hilbert space at different points (r_m, t_m) are not orthogonal to each other. In our treatment here, we linear transform $c_{r_m}(t_m), c_{r_m}(t_m)^\dagger$ into an orthogonal fermion basis Eq. (6) (which requires free fermion Hamiltonian), and then define the tensor product of their Hilbert spaces as the sub-Hilbert space h_A of slice A , which ensures h_A to be a well-defined subspace of the physical Hilbert space. In temporal entanglement of tensor networks, such an orthogonalization of the local Hilbert spaces at different spacetime points (r_m, t_m) is absent (thus not requiring free Hamiltonian), and the basis of spatial transfer matrix is regarded as the sub-Hilbert space of slice A , which is however not a subspace of the physical Hilbert space. This difference in definitions leads to different resulting entanglement entropy behaviors.

The entanglement spectrum [54] and operators in entanglement Hamiltonian [55] of the timelike reduced density matrix in our formalism await future studies. The generalization of spacetime entanglement entropy into interacting models is also a challenging question. A simple generalization is to define the spacetime entanglement entropy in the interaction picture in the method formulated in this paper. Namely, for Hamiltonian $H = H_0 + H_I$ where H_0 is a free fermion Hamiltonian and H_I is interaction, we can consider operators in the interaction picture

$$O_{\mathbf{r},j}^{(I)}(t) = e^{iH_0 t} O_{\mathbf{r},j} e^{-iH_0 t} \quad (47)$$

at coordinates (\mathbf{r}, t) in spacetime slice A , and define the sub-Hilbert space h_A as the minimal subspace in which n -point functions within slice A are calculable (similar to Eq. (3)):

$$\langle \prod_{\alpha \in A} O_{\mathbf{r}_{n_\alpha}, j_\alpha}^{(I)}(t_{n_\alpha}) \rangle = \text{tr} \left[\rho_A \prod_{\alpha \in A} O_{\mathbf{r}_{n_\alpha}, j_\alpha}^{(I)}(t_{n_\alpha}) \right], \quad (48)$$

where ρ_A is the corresponding reduced density matrix. In this way, identification of the sub-Hilbert space h_A of slice A follows the same procedure as Sec. II A with H replaced by H_0 . The only difference is that the quantum states are no longer time-independent, but is evolved by the interaction. Accordingly, the calculation of entanglement

entropy becomes much more difficult. We leave the study of such interacting systems to the future.

Acknowledgments

Acknowledgments. We thank Ying Zhao, J. Alexander Jacoby and Xiao-Liang Qi for helpful conversations. This work is supported by the Alfred P. Sloan Foundation, the National Science Foundation through Princeton University's Materials Research Science and Engineering Center DMR-2011750, and the National Science Foundation under award DMR-2141966. Additional support is provided by the Gordon and Betty Moore Foundation through Grant GBMF8685 towards the Princeton theory program.

-
- [1] R. Horodecki and P. Horodecki, Quantum redundancies and local realism, *Physics Letters A* **194**, 147 (1994).
 - [2] M. Horodecki, P. Horodecki, and R. Horodecki, Separability of mixed states: necessary and sufficient conditions, *Physics Letters A* **223**, 1 (1996).
 - [3] N. J. Cerf and C. Adami, Negative entropy and information in quantum mechanics, *Phys. Rev. Lett.* **79**, 5194 (1997).
 - [4] R. Horodecki, P. Horodecki, M. Horodecki, and K. Horodecki, Quantum entanglement, *Rev. Mod. Phys.* **81**, 865 (2009).
 - [5] A. Einstein, B. Podolsky, and N. Rosen, Can quantum-mechanical description of physical reality be considered complete?, *Phys. Rev.* **47**, 777 (1935).
 - [6] N. Bohr, Can quantum-mechanical description of physical reality be considered complete?, *Phys. Rev.* **48**, 696 (1935).
 - [7] J. S. Bell, On the einstein podolsky rosen paradox, *Physics Physique Fizika* **1**, 195 (1964).
 - [8] L. Bombelli, R. K. Koul, J. Lee, and R. D. Sorkin, Quantum source of entropy for black holes, *Phys. Rev. D* **34**, 373 (1986).
 - [9] M. Srednicki, Entropy and area, *Phys. Rev. Lett.* **71**, 666 (1993).
 - [10] M. B. Hastings, Entropy and entanglement in quantum ground states, *Phys. Rev. B* **76**, 035114 (2007).
 - [11] J. Eisert, M. Cramer, and M. B. Plenio, Colloquium: Area laws for the entanglement entropy, *Rev. Mod. Phys.* **82**, 277 (2010).
 - [12] J. L. Cardy and I. Peschel, Finite-size dependence of the free energy in two-dimensional critical systems, *Nuclear Physics B* **300**, 377 (1988).
 - [13] P. Calabrese and J. Cardy, Entanglement entropy and quantum field theory, *Journal of Statistical Mechanics: Theory and Experiment* **2004**, P06002 (2004).
 - [14] P. Calabrese and J. Cardy, Entanglement entropy and conformal field theory, *Journal of Physics A: Mathematical and Theoretical* **42**, 504005 (2009).
 - [15] D. Gioev and I. Klich, Entanglement entropy of fermions in any dimension and the widom conjecture, *Phys. Rev. Lett.* **96**, 100503 (2006).
 - [16] M. M. Wolf, Violation of the entropic area law for fermions, *Phys. Rev. Lett.* **96**, 010404 (2006).
 - [17] M. Cramer, J. Eisert, and M. B. Plenio, Statistics dependence of the entanglement entropy, *Phys. Rev. Lett.* **98**, 220603 (2007).
 - [18] W. Li, L. Ding, R. Yu, T. Roscilde, and S. Haas, Scaling behavior of entanglement in two- and three-dimensional free-fermion systems, *Phys. Rev. B* **74**, 073103 (2006).
 - [19] T. Barthel, M.-C. Chung, and U. Schollwöck, Entanglement scaling in critical two-dimensional fermionic and bosonic systems, *Phys. Rev. A* **74**, 022329 (2006).
 - [20] A. Kitaev and J. Preskill, Topological entanglement entropy, *Phys. Rev. Lett.* **96**, 110404 (2006).
 - [21] M. Levin and X.-G. Wen, Detecting topological order in a ground state wave function, *Phys. Rev. Lett.* **96**, 110405 (2006).
 - [22] B. Bauer and C. Nayak, Area laws in a many-body localized state and its implications for topological order, *Journal of Statistical Mechanics: Theory and Experiment* **2013**, 09005 (2013), arXiv:1306.5753 [cond-mat.dis-nn].
 - [23] D. A. Huse, R. Nandkishore, V. Oganesyan, A. Pal, and S. L. Sondhi, Localization-protected quantum order, *Phys. Rev. B* **88**, 014206 (2013).
 - [24] R. V. Jensen and R. Shankar, Statistical behavior in deterministic quantum systems with few degrees of freedom, *Phys. Rev. Lett.* **54**, 1879 (1985).
 - [25] J. M. Deutsch, Quantum statistical mechanics in a closed system, *Phys. Rev. A* **43**, 2046 (1991).
 - [26] M. Srednicki, Chaos and quantum thermalization, *Phys. Rev. E* **50**, 888 (1994).
 - [27] J. D. Bekenstein, Black holes and entropy, *Phys. Rev. D* **7**, 2333 (1973).
 - [28] S. W. Hawking, Particle creation by black holes, *Communications In Mathematical Physics* **43**, 199 (1975).
 - [29] L. Bombelli, R. K. Koul, J. Lee, and R. D. Sorkin, Quantum source of entropy for black holes, *Phys. Rev. D* **34**, 373 (1986).
 - [30] R. Bousso, The holographic principle, *Rev. Mod. Phys.* **74**, 825 (2002).
 - [31] A. J. Leggett and A. Garg, Quantum mechanics versus macroscopic realism: Is the flux there when nobody looks?, *Phys. Rev. Lett.* **54**, 857 (1985).
 - [32] J. P. Paz and G. Mahler, Proposed test for temporal bell

- inequalities, *Phys. Rev. Lett.* **71**, 3235 (1993).
- [33] S. Taylor, S. Cheung, Č. Brukner, and V. Vedral, Entanglement in time and temporal communication complexity, *AIP Conference Proceedings* **734**, 281 (2004), <https://aip.scitation.org/doi/pdf/10.1063/1.1834435>.
 - [34] O. Oreshkov, F. Costa, and Č. Brukner, Quantum correlations with no causal order, *Nature Communications* **3**, 1092 (2012), [arXiv:1105.4464 \[quant-ph\]](https://arxiv.org/abs/1105.4464).
 - [35] J. Fitzsimons, J. Jones, and V. Vedral, Quantum correlations which imply causation, *arXiv e-prints*, [arXiv:1302.2731](https://arxiv.org/abs/1302.2731) (2013), [arXiv:1302.2731 \[quant-ph\]](https://arxiv.org/abs/1302.2731).
 - [36] Č. Brukner, Quantum causality, *Nature Physics* **10**, 259 (2014).
 - [37] K. Ried, M. Agnew, L. Vermeyden, D. Janzing, R. W. Spekkens, and K. J. Resch, A quantum advantage for inferring causal structure, *Nature Physics* **11**, 414 (2015), [arXiv:1406.5036 \[quant-ph\]](https://arxiv.org/abs/1406.5036).
 - [38] Č. Brukner, Bounding quantum correlations with indefinite causal order, *New Journal of Physics* **17**, 083034 (2015), [arXiv:1404.0721 \[quant-ph\]](https://arxiv.org/abs/1404.0721).
 - [39] D. Jia, Generalizing entanglement, *Phys. Rev. A* **96**, 062132 (2017).
 - [40] J. Cotler, C.-M. Jian, X.-L. Qi, and F. Wilczek, Superdensity operators for spacetime quantum mechanics, *Journal of High Energy Physics* **2018**, 93 (2018), [arXiv:1711.03119 \[quant-ph\]](https://arxiv.org/abs/1711.03119).
 - [41] J. Cotler, X. Han, X.-L. Qi, and Z. Yang, Quantum causal influence, *Journal of High Energy Physics* **2019**, 42 (2019), [arXiv:1811.05485 \[hep-th\]](https://arxiv.org/abs/1811.05485).
 - [42] E. Gillman, F. Carollo, and I. Lesanovsky, Quantum and classical temporal correlations in (1 + 1)D quantum cellular automata, *Phys. Rev. Lett.* **127**, 230502 (2021).
 - [43] T. M. Nebabu and X. Qi, Bulk reconstruction from generalized free fields (2023), [arXiv:2306.16687 \[hep-th\]](https://arxiv.org/abs/2306.16687).
 - [44] A. Leroose, M. Sonner, and D. A. Abanin, Influence matrix approach to many-body floquet dynamics, *Phys. Rev. X* **11**, 021040 (2021).
 - [45] A. Leroose, M. Sonner, and D. A. Abanin, Scaling of temporal entanglement in proximity to integrability, *Phys. Rev. B* **104**, 035137 (2021).
 - [46] M. Sonner, A. Leroose, and D. A. Abanin, Influence functional of many-body systems: Temporal entanglement and matrix-product state representation, *Annals of Physics* **435**, 168677 (2021), special issue on Philip W. Anderson.
 - [47] G. Giudice, G. Giudici, M. Sonner, J. Thoenness, A. Leroose, D. A. Abanin, and L. Piroli, Temporal entanglement, quasiparticles, and the role of interactions, *Phys. Rev. Lett.* **128**, 220401 (2022).
 - [48] R. Feynman and F. Vernon, The theory of a general quantum system interacting with a linear dissipative system, *Annals of Physics* **24**, 118 (1963).
 - [49] A. Müller-Hermes, J. I. Cirac, and M. C. Bañuls, Tensor network techniques for the computation of dynamical observables in one-dimensional quantum spin systems, *New Journal of Physics* **14**, 075003 (2012).
 - [50] M. B. Hastings and R. Mahajan, Connecting entanglement in time and space: Improving the folding algorithm, *Phys. Rev. A* **91**, 032306 (2015).
 - [51] See Supplemental Material for details.
 - [52] I. Peschel, Calculation of reduced density matrices from correlation functions, *Journal of Physics A: Mathematical and General* **36**, L205 (2003).
 - [53] E. H. Lieb and D. W. Robinson, The finite group velocity of quantum spin systems, *Communications in Mathematical Physics* **28**, 251 (1972).
 - [54] H. Li and F. D. M. Haldane, Entanglement spectrum as a generalization of entanglement entropy: Identification of topological order in non-abelian fractional quantum hall effect states, *Phys. Rev. Lett.* **101**, 010504 (2008).
 - [55] B. Lian, Conserved quantities from entanglement hamiltonian, *Phys. Rev. B* **105**, 035106 (2022).

Supplemental Material for “Entanglement Entropy of Free Fermions in Timelike Slices”

Bowei Liu, Hao Chen, and Biao Lian
December 19, 2023

I. Fermion Operator Orthonormalization

We give the details of orthonormalizing the free fermion creation and annihilation operators in an arbitrary spacetime slice A in this section. Consider the full system with a total number of fermion modes L . Given K single-particle annihilation operators $c_{\mathbf{r}_1}(t_1), c_{\mathbf{r}_2}(t_2), \dots, c_{\mathbf{r}_K}(t_K)$ in slice A , we can express them as

$$c_{\mathbf{r}_j}(t_j) = e^{iHt_n} c_{\mathbf{r}_j} e^{-iHt_n} = \sum_l a_l \phi_{l,\mathbf{r}_j} e^{-i\varepsilon_l t_j}, \quad (\text{S1})$$

where ϕ_{l,\mathbf{r}_j} is the l -th ($1 \leq l \leq L$) single-particle eigenstate wave function (normalized) of the full system, a_l is the l -th single-particle eigenstate annihilation operator, and ε_l are the energy of the l -th single-particle eigenstate. In the case that the lattice model has one fermion mode per site and has the translation symmetry (which is the case we study in this paper), the eigenfunctions are simply plane waves:

$$\phi_{l,\mathbf{r}_j} = \frac{1}{\sqrt{L}} e^{i\mathbf{k}_l \cdot \mathbf{r}_j}, \quad (\text{S2})$$

where \mathbf{k}_l is the quasi-momentum of the l -th single-particle eigenstate. Define the $K \times L$ matrix ϕ^A as

$$\phi_{jl}^A = \phi_{l,\mathbf{r}_j} e^{-i\varepsilon_l t_j}, \quad 1 \leq j \leq K, \quad 1 \leq l \leq L. \quad (\text{S3})$$

The anticommutator matrix in slice A is then:

$$B_{mn} = \{c_{\mathbf{r}_m}(t_m), c_{\mathbf{r}_n}^\dagger(t_n)\} = \sum_l \phi_{l,\mathbf{r}_m} \phi_{l,\mathbf{r}_n}^* e^{-i\varepsilon_l(t_m - t_n)} = (\phi^A \phi^{A\dagger})_{mn}, \quad 1 \leq m \leq K, \quad 1 \leq n \leq K. \quad (\text{S4})$$

The $\{c_{\mathbf{r}_j}(t_j)\}$ operators no longer serve as an orthonormal fermion operator basis because B_{mn} is not the identity matrix. To find an orthonormal fermion operator basis, we notice that B is Hermitian and positive semi-definite. *Assuming B is full rank* (if not full rank, one can work with the full rank part of B , see the section “Definition of δ cutoff”), there exists $K \times K$ matrix M such that

$$M^\dagger M = B^{-1}. \quad (\text{S5})$$

In general, M is not unique. Here we choose to diagonalize B as $B = Q\Lambda Q^\dagger$, where Λ is diagonal and Q is unitary, and we then define the matrix $M = \Lambda^{-1/2} Q^\dagger$. Then we can introduce new operators $d_m = \sum_{n \in A} M_{mn} c_n(t_n)$ which are canonically orthonormalized:

$$\{d_m, d_n^\dagger\} = \sum_{j,l} M_{mj} M_{ln}^\dagger \{c_{\mathbf{r}_j}(t_j), c_{\mathbf{r}_l}^\dagger(t_l)\} = \sum_{j,l} M_{mj} (M^\dagger M)_{jl}^{-1} M_{ln}^\dagger = \delta_{mn}. \quad (\text{S6})$$

By defining

$$c = \begin{bmatrix} c_{\mathbf{r}_1}(t_1) \\ c_{\mathbf{r}_2}(t_2) \\ \vdots \\ c_{\mathbf{r}_K}(t_K) \end{bmatrix}, \quad a = \begin{bmatrix} a_1 \\ a_2 \\ \vdots \\ a_L \end{bmatrix}, \quad d = \begin{bmatrix} d_1 \\ d_2 \\ \vdots \\ d_K \end{bmatrix}, \quad (\text{S7})$$

we can rewrite the transformation in matrix form as

$$c = \phi^A a, \quad d = M c = M \phi^A a. \quad (\text{S8})$$

The correlation matrices satisfy

$$D_{mn} = \text{tr}(\rho_{\text{tot}} d_m^\dagger d_n) = \sum_{j,l} M_{nl} M_{mj}^* \text{tr}(\rho_{\text{tot}} c_{\mathbf{r}_j}^\dagger(t_j) c_{\mathbf{r}_l}(t_l)) = (M^* C M^T)_{mn}, \quad m, n \in A. \quad (\text{S9})$$

For a time-direction slice shown in the main text Fig. 1b, every operator sits at site 0 but are at different time t_n . So we only need to substitute

$$c = \begin{bmatrix} c_{\mathbf{r}_0}(t_1) \\ c_{\mathbf{r}_0}(t_2) \\ \vdots \\ c_{\mathbf{r}_0}(t_K) \end{bmatrix}, \quad \phi_{jl}^A = \phi_{l,0} e^{-i\varepsilon_l t_j}, \quad (\text{S10})$$

into Eqs. (S4), (S5) and (S8) to define fermion basis d .

II. Comparison with the Temporal Entanglement Entropy for Influence Matrix

Here we comment on the differences between the spacetime slice entanglement entropy we defined in this paper and the temporal entanglement entropy for influence matrix studied in [44–48].

The influence matrix setup considers quantum systems (circuits, etc.) at discrete times $t_n = n\tau$. In the example of fermions, the influence matrix on a fixed site $m = 0$ takes the form

$$\mathcal{F}(\{\sigma_0, \sigma_\tau, \dots, \sigma_{n\tau}, \dots; \bar{\sigma}_0, \bar{\sigma}_\tau, \dots, \bar{\sigma}_{n\tau}, \dots\}), \quad \sigma_{n\tau}, \bar{\sigma}_{n\tau} \in \{0, 1\}, \quad (\text{S11})$$

which is understood as the quantum amplitude that the density matrix $\rho_{\text{tot}}(n\tau) = e^{-iHn\tau} \rho_{\text{tot}} e^{iHn\tau}$ at time $t = n\tau$ is locally in the state $|\sigma_{n\tau}\rangle \langle \bar{\sigma}_{n\tau}|_{m=0}$, where $|0\rangle_m$ and $|1\rangle_m$ are the unoccupied and occupied fermion state on site m at time $n\tau$. Or in the notations of our paper, $c_m^\dagger(n\tau)c_m(n\tau)|\sigma_{n\tau}\rangle_m = \sigma_{n\tau}|\sigma_{n\tau}\rangle_m$ for $\sigma_{n\tau} = 0$ or 1, where $c_m(n\tau) = e^{-iHt}c_m e^{iHt}$ and $c_m^\dagger(n\tau) = e^{-iHt}c_m^\dagger e^{iHt}$. More explicitly, the influence matrix satisfies

$$\prod_{n' \neq n} \sum_{\sigma_{n'\tau} = \bar{\sigma}_{n'\tau}} \mathcal{F}(\{\sigma_{n\tau}; \bar{\sigma}_{n\tau}\}) = \text{tr}(\rho_{\text{tot}}(n\tau)|\sigma_{n\tau}\rangle \langle \bar{\sigma}_{n\tau}|_{m=0}). \quad (\text{S12})$$

The temporal entanglement entropy for influence matrix $\mathcal{F}(\{\sigma_{n\tau}; \bar{\sigma}_{n\tau}\})$ is defined by treating $\mathcal{F}(\{\sigma_{n\tau}; \bar{\sigma}_{n\tau}\})$ in Eq. (S11) as a “wavefunction” in a doubled time “Fock basis”:

$$|\sigma_0, \sigma_\tau, \dots, \sigma_{n\tau}, \dots, \bar{\sigma}_0, \bar{\sigma}_\tau, \dots, \bar{\sigma}_{n\tau}, \dots\rangle_{m=0}, \quad (\text{S13})$$

and calculate the entanglement entropy S_A^{temp} of this “wavefunction” in a time interval t in the usual sense.

This temporal entanglement entropy S_A^{temp} above is by definition a different concept from our time direction entanglement entropy S_A in this paper, which we explain below.

1) Since the influence matrix is an operator, S_A^{temp} is calculated by mapping it into a “state” in the operator space, and thus S_A^{temp} is a characterization of operator entanglement. In contrast, our time-direction entanglement entropy S_A is calculated for a sub-Hilbert space h_A of the physical quantum state, which is a characterization of state entanglement. For a slice A of time interval t containing K points, S_A^{temp} is calculated in an operator sub-Hilbert space of dimension 2^{2K} , while our S_A is calculated in a state sub-Hilbert space h_A of dimension 2^K .

2) In the definition of S_A^{temp} , an effective doubled Fock basis in Eq. (S13) is defined. However, two states $|\sigma_{n\tau}\rangle_m$ and $|\sigma_{n'\tau}\rangle_m$ at different times $n\tau$ and $n'\tau$ ($n \neq n'$) are not orthogonal in the physical Hilbert space, since $\{c_m(n\tau), c_m^\dagger(n'\tau)\} \neq 0$ as we explained in the main text. Therefore, the doubled Fock basis, defined in Eq. (S13) as direct product of states $|\sigma_{n\tau}\rangle_m$ at different times, do not correspond to a physical state in the physical doubled Hilbert space. In contrast, in our definition of time-direction entanglement entropy S_A , an orthogonal physical Fock basis is defined by transforming the fermion operators $c_m(n\tau)$ into an orthogonal fermion basis d_m as defined in main text Eq. (3), so S_A does correspond to the entanglement entropy of a physical state in a physical sub-Hilbert space.

3) Given the above differences in the definitions of S_A^{temp} and S_A , they do show different behaviors numerically. As shown in [47], in both non-interacting fermion models and interacting models, the influence matrix temporal entanglement entropy S_A^{temp} at infinite temperature (or for high energy states) is sublinear in time t , and in many cases shows area law in t . In contrast, in our paper, we showed that the time-direction entanglement entropy S_A is linear in time t (namely, volume law) at any finite temperature when $\tau < \tau_0$ (Fig. S7). These two results are thus clearly different. This is because the temporal entanglement entropy S_A^{temp} detects the entanglement of operators, which is low (less correlated) at high temperatures; while our time-direction entanglement entropy S_A detects the entanglement of states, which show volume law at high temperatures/energies.

An entropy along the time direction has also been defined for tensor networks by transverse contractions and folding algorithms [49, 50], similar to that of the influence matrix. Similarly, it (at least) has the significant distinction from

our entanglement entropy that, its basis at different times are implicitly regarded as orthogonal and used to form a direct product Fock basis (similar to the second point above). We do note that for fixed $\tau \gg \tau_0$, the main text Eq. (9) indicates that our zero temperature time-direction entanglement entropy $S_A = K[-\nu \ln \nu - (1 - \nu) \ln(1 - \nu)]$ is linear in time $t = (K - 1)\tau$, which is similar to the linear-in- t temporal entanglement entropy without folding in [49, 50]. We conjecture this is because, in the limit $\tau \gg \tau_0$, the fermion basis $c_m(n\tau)$ at different times $n\tau$ become approximately orthogonal, and our Fock basis approximately agrees with that used in [49, 50].

We leave the understanding of the underlying connection between the influence matrix S_A^{temp} and our S_A to future studies.

III. Alternative Fermion Dispersions

We consider the following four dispersion relations of 1D free fermions:

$$\text{cosine dispersion (the tight-binding model in main text): } E(k) = -\frac{E_0}{2} \cos(ka_0) \quad (\text{S14})$$

$$\text{quadratic dispersion } (k^2): \quad E(k) = -\frac{E_0}{2} \left(1 - \frac{2(ka_0)^2}{\pi^2}\right) \quad (\text{S15})$$

$$\text{nonchiral linear dispersion: } E(k) = -\frac{E_0}{2} \left(1 - \frac{2|ka_0|}{\pi}\right) \quad (\text{S16})$$

$$\text{chiral linear dispersion: } E(k) = \frac{E_0}{2} \frac{ka_0}{\pi} \quad (\text{S17})$$

In particular, the results presented in the main text are all for the cosine dispersion in Eq. (S14), or the model in main text Eq. (7). The range of energy spectrum is E_0 for all the four dispersion relations, such that they have the same characteristic time $\tau_0 = 2\pi/E_0$, see Fig. S1a. Fig. S1b shows the fixed t zero-temperature entanglement entropy S_A calculated for these energy dispersions, which are similar except for the trapezoid plateaus of the curves.

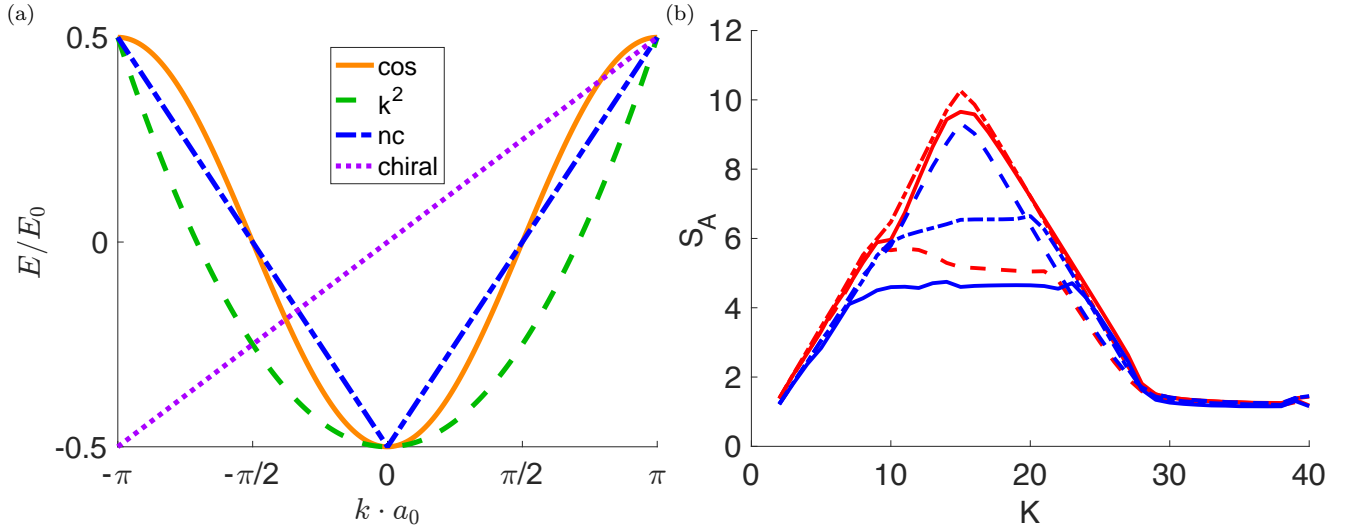


FIG. S1. (a) Cosine dispersion Eq. (S14), quadratic (k^2) dispersion Eq. (S15), nonchiral (nc) linear dispersion Eq. (S16), and chiral linear dispersion Eq. (S17). (b) Zero temperature S_A in time-direction slice with fixed $2\pi t/\tau_0 = 168$ at $\nu = 0.5$ (red) and $\nu = 0.7$ (blue) for different fermion dispersions in (a): the cosine (solid lines), quadratic (dashed lines), nonchiral linear and chiral linear (which have equal S_A , dashed-dotted lines).

IV. Scaling Behavior and Oscillation Period at $\tau \leq \tau_0$

We now show the scaling behavior and oscillation period of the zero-temperature entanglement entropy S_A in the time-direction slice with fixed time separation $\tau = \tau_0, \frac{2}{\pi}\tau_0$ or $\frac{1}{2}\tau_0$. For $\tau \leq \tau_0$, the zero temperature S_A is in general a linear function in $\ln K$ plus an oscillation in K . The oscillation amplitude is small when $\tau = \tau_0$ (Fig. S2), but is large when $\tau \ll \tau_0$ (Figs. S3 and S4). We first fit a linear function $S_{\text{fit}} = a \cdot \ln(K) + b$ to extract $a = \left(\frac{\partial S_A}{\partial \ln(K)} \right)_\tau$. Then we find the oscillation period of $S_A - S_{\text{fit}}$ (using the fitted parameters a and b) against K . The oscillation is periodic in K . To mitigate the effect of oscillation to the fitting, we have excluded the entropy at small K , see captions of Tabs. I to III. The number of filled single-fermion eigenstates are 101, 151, 201, 251, 301, 351 for $\nu = 0.2, 0.3, 0.4, 0.5, 0.6, 0.7$ respectively (total size $L = 500$), to avoid breaking the double degeneracy in the cases of cosine, k^2 , and nonchiral spectrum in Eqs. (S14) to (S16). The nonchiral spectrum in Eq. (S16) gives almost the same entanglement entropy as chiral spectrum in Eq. (S17) due to their nearly identical density of states $\Omega(E)$, so we have only plotted the entanglement entropy of the cosine, k^2 and chiral spectra in Figs. S2 to S4.

As shown in Tabs. I to III, $\left(\frac{\partial S_A}{\partial \ln(K)} \right)_\tau$ is about $\frac{1}{3}$ at $\tau = \tau_0$, whereas $\left(\frac{\partial S_A}{\partial \ln(K)} \right)_\tau$ is around $\frac{1}{6}$ at $\tau = \frac{2}{\pi}\tau_0$ or $\tau = \frac{1}{2}\tau_0$. This result is independent of filling ν or dispersion relations.

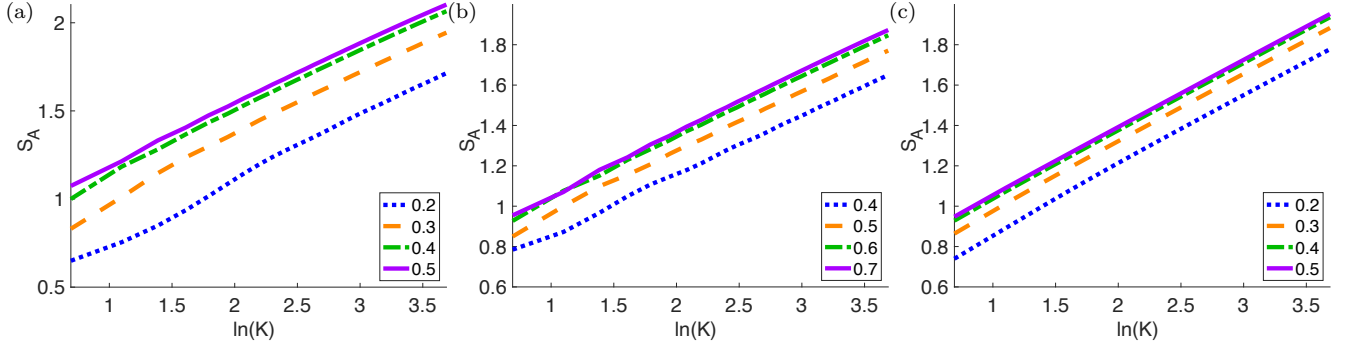


FIG. S2. Zero temperature entanglement entropy S_A versus $\ln K$ in time direction slice for different fillings ν (see legend) at fixed $\tau = \tau_0$ for (a) cosine dispersion Eq. (S14), (b) quadratic dispersion Eq. (S15), and (c) chiral linear dispersion Eq. (S17).

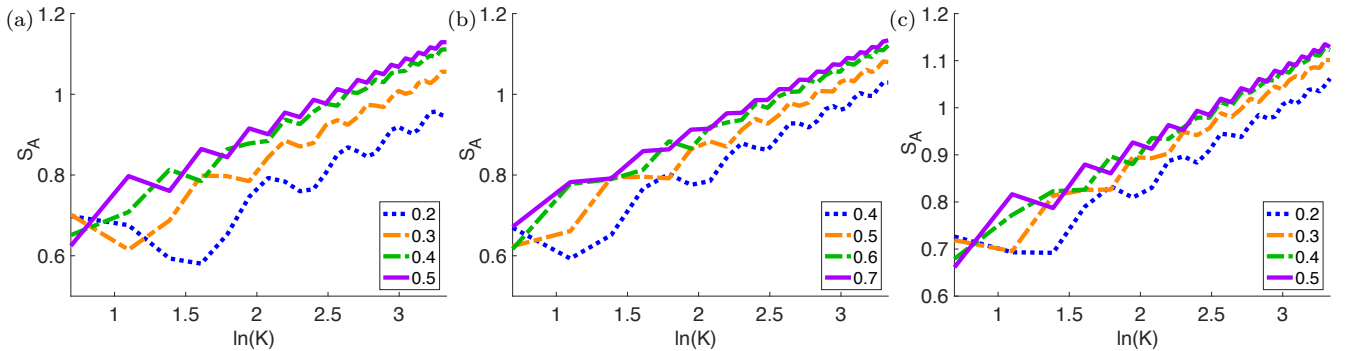


FIG. S3. Zero temperature entanglement entropy S_A versus $\ln K$ in time direction slice for different fillings ν (see legend) at fixed $\tau = \frac{2}{\pi}\tau_0$ for (a) cosine dispersion Eq. (S14), (b) quadratic dispersion Eq. (S15), and (c) chiral linear dispersion Eq. (S17).

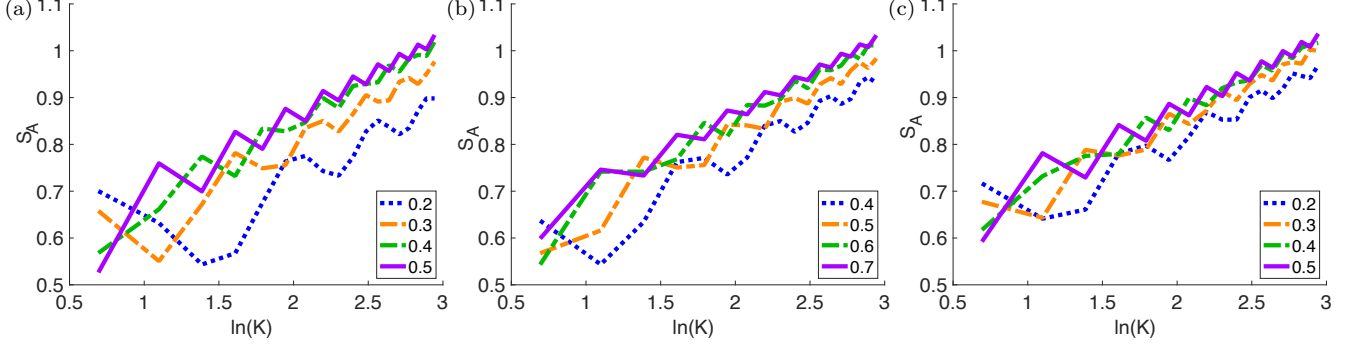


FIG. S4. Zero temperature entanglement entropy S_A versus $\ln K$ in time direction slice for different fillings ν (see legend) at fixed $\tau = \tau_0/2$ for (a) cosine dispersion Eq. (S14), (b) quadratic dispersion Eq. (S15), and (c) chiral linear dispersion Eq. (S17).

ν	$\left(\frac{\partial S_A}{\partial \ln(K)}\right)_\tau$ at $\tau = \tau_0$	period at $\tau = \tau_0$	$\left(\frac{\partial S_A}{\partial \ln(K)}\right)_\tau$ at $\tau = \frac{2}{\pi}\tau_0$	period at $\tau = \frac{2}{\pi}\tau_0$	$\left(\frac{\partial S_A}{\partial \ln(K)}\right)_\tau$ at $\tau = \frac{1}{2}\tau_0$	period at $\tau = \frac{1}{2}\tau_0$
0.2	0.3423 ± 0.0022	9.0	0.1606 ± 0.0310	5.7	0.1979 ± 0.0483	5.5
0.3	0.3317 ± 0.0017	4.5	0.1638 ± 0.0179	3.7	0.1649 ± 0.0310	3.3
0.4	0.3273 ± 0.0018	3.0	0.1667 ± 0.0133	2.6	0.1843 ± 0.0247	2.4
0.5	0.3261 ± 0.0020	2.0	0.1697 ± 0.0158	2.0	0.1677 ± 0.0291	2.0

TABLE I. In time direction slice with cosine dispersion Eq. (S14), 95% confidence bound of $\left(\frac{\partial S_A}{\partial \ln(K)}\right)_\tau$ is fitted from the zero temperature entanglement entropy S_A at $K \in [11, 40], [12, 28], [5, 19]$ when fixing $\tau = \tau_0, \frac{2}{\pi}\tau_0, \frac{1}{2}\tau_0$, respectively.

ν	$\left(\frac{\partial S_A}{\partial \ln(K)}\right)_\tau$ at $\tau = \tau_0$	period at $\tau = \tau_0$	$\left(\frac{\partial S_A}{\partial \ln(K)}\right)_\tau$ at $\tau = \frac{2}{\pi}\tau_0$	period at $\tau = \frac{2}{\pi}\tau_0$	$\left(\frac{\partial S_A}{\partial \ln(K)}\right)_\tau$ at $\tau = \frac{1}{2}\tau_0$	period at $\tau = \frac{1}{2}\tau_0$
0.2	0.3411 ± 0.0024	∞	0.1511 ± 0.0136	3.6	0.1438 ± 0.0275	3.7
0.3	0.3362 ± 0.0015	∞	0.1594 ± 0.0094	2.9	0.1594 ± 0.0194	2.8
0.4	0.3340 ± 0.0009	∞	0.1644 ± 0.0059	2.3	0.1685 ± 0.0131	2.3
0.5	0.3335 ± 0.0007	∞	0.1660 ± 0.0102	2.0	0.1724 ± 0.0232	2.0

TABLE II. In time direction slice with chiral linear dispersion Eq. (S17), 95% confidence bound of $\left(\frac{\partial S_A}{\partial \ln(K)}\right)_\tau$ is fitted from the zero temperature entanglement entropy S_A at $K \in [2, 40], [2, 28], [2, 19]$ when fixing $\tau = \tau_0, \frac{2}{\pi}\tau_0, \frac{1}{2}\tau_0$, respectively.

ν	$\left(\frac{\partial S_A}{\partial \ln(K)}\right)_\tau$ at $\tau = \tau_0$	period at $\tau = \tau_0$	$\left(\frac{\partial S_A}{\partial \ln(K)}\right)_\tau$ at $\tau = \frac{2}{\pi}\tau_0$	period at $\tau = \frac{2}{\pi}\tau_0$	$\left(\frac{\partial S_A}{\partial \ln(K)}\right)_\tau$ at $\tau = \frac{1}{2}\tau_0$	period at $\tau = \frac{1}{2}\tau_0$
0.4	0.2926 ± 0.0021	5.8	0.1638 ± 0.0156	4.2	0.1909 ± 0.0294	4.3
0.5	0.2992 ± 0.0025	3.8	0.1720 ± 0.0091	3.3	0.1751 ± 0.0242	3.3
0.6	0.3015 ± 0.0019	2.7	0.1728 ± 0.0092	2.6	0.1618 ± 0.0171	2.5
0.7	0.3054 ± 0.0022	2.0	0.1684 ± 0.0055	2.0	0.1651 ± 0.0160	2.0

TABLE III. In time direction slice with quadratic dispersion relation Eq. (S15), 95% confidence bound of $\left(\frac{\partial S_A}{\partial \ln(K)}\right)_\tau$ is fitted from the zero temperature entanglement entropy S_A at $K \in [2, 40], [2, 28], [3, 19]$ when fixing $\tau = \tau_0, \frac{2}{\pi}\tau_0, \frac{1}{2}\tau_0$, respectively.

V. Entanglement Entropy in the Plateau

In the main text Fig. 2a, we have shown the time-direction entanglement entropy shows a trapezoid shape with a plateau or triangular shape when $K < t/\tau_0$, depending on filling ν . Fig. S5 here shows the maximal entanglement entropy S_A (occurring in the trapezoid plateau or the triangle top vertex) in the range of $K < t/\tau_0$ in a fixed t zero temperature time-direction slice (normalized by the maximal possible S_A), with respect to the Fermi energy $E_F \in [-\frac{E_0}{2}, \frac{E_0}{2}]$. The curve of S_A forms a triangle with respect to Fermi energy E_F , which is almost independent of dispersion relation, suggesting the plateau entropy only depends on E_F (instead of filling ν).

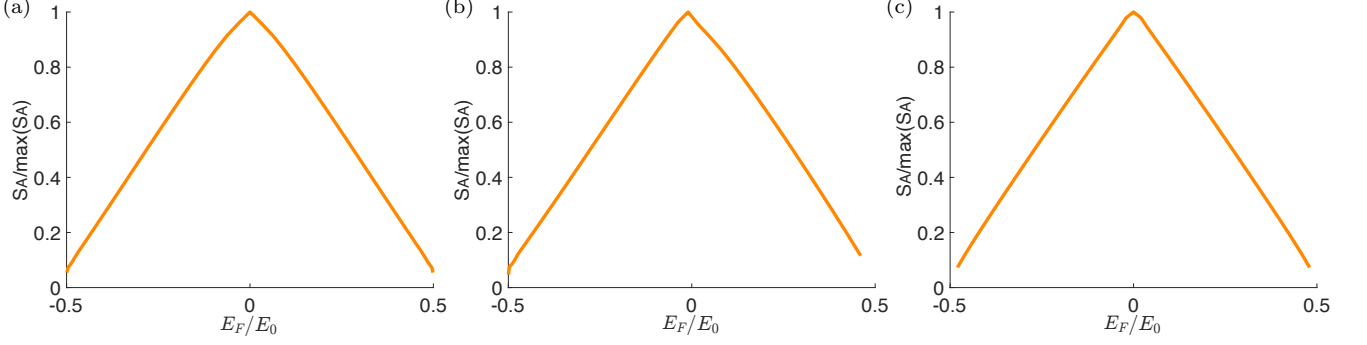


FIG. S5. At fixed $2\pi t/\tau_0 = 168$ and $K = 15$ ($\tau \approx 2\tau_0$) in a time direction slice, zero temperature entanglement entropy S_A is at the tip of the triangle when $E_F = 0$ or middle of the plateau when $E_F \neq 0$. This plateau entanglement entropy S_A normalized by the tip of the triangle $\max(S_A)$ (entropy S_A when $E_F = 0$) is given for (a) cosine dispersion Eq. (S14), (b) quadratic dispersion Eq. (S15), and (c) chiral linear dispersion Eq. (S17) (which is the same as nonchiral linear dispersion Eq. (S16)), respectively. Note that $E_F = 0$ corresponds to filling $\nu = 0.5$ for cosine and chiral/nonchiral linear dispersions, and $\nu \approx 0.7$ for quadratic dispersion.

VI. t Dependence at Finite Temperature

Fig. S6 shows that in a time direction slice, $(\frac{\partial S_A}{\partial K})_t$ at $K \gg t/\tau_0$ ($\tau \ll \tau_0$) with fixed t is almost independent of t , regardless of temperature T .

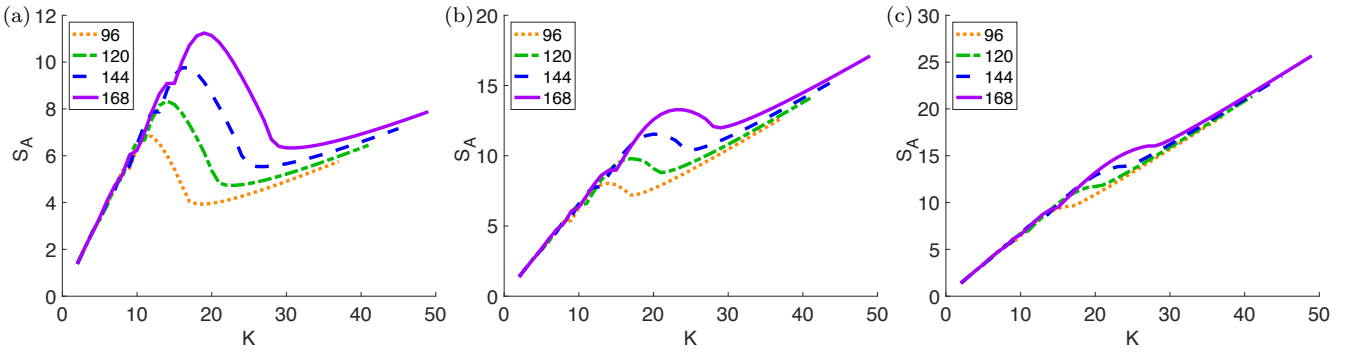


FIG. S6. Time-direction slice entanglement entropy S_A of model Eq. (S14) at fixed filling $\nu = 0.5$ and finite temperature $T/E_0 = 0.0625, 0.1375, 0.25$ is shown in (a), (b), (c), respectively. In each panel, different values of $2\pi t/\tau_0$ is given in the legend. Each curve is kept up to a reliable value of K , since numerical accuracy becomes insufficient for larger K .

When we fix time separation $\tau < \tau_0$, we get a volume law $S_A \propto t$ at finite temperature, see Fig. S7.

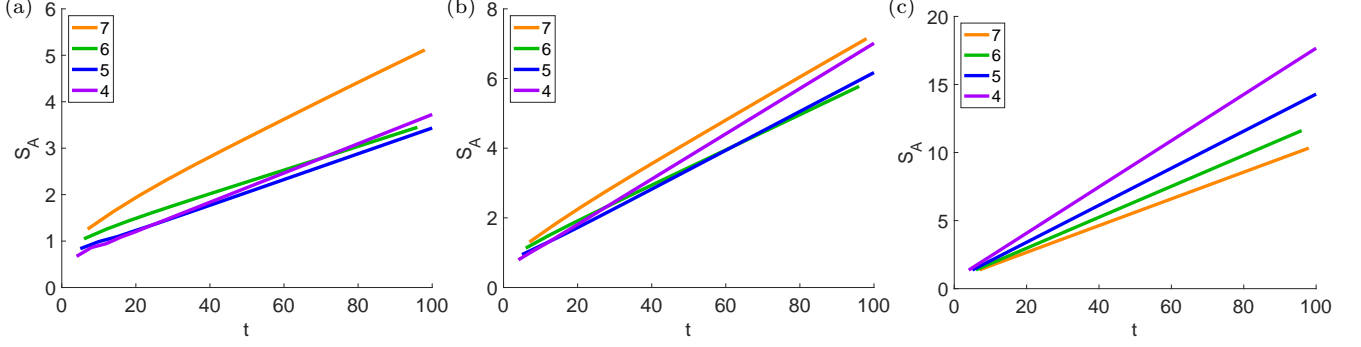


FIG. S7. Time-direction slice entanglement entropy S_A of model Eq. (S14) with fixed time spacing τ at fixed filling $\nu = 0.5$, $\delta = 10^{-18}$, and finite temperature $T/E_0 = 0.05, 0.1, 1$ is shown in (a), (b), (c), respectively. In each panel, different values of $2\pi\tau/\tau_0$ is given in the legend.

VII. Entanglement Entropy in Linear Slice with Large θ

Fig. S8 shows that the zero temperature entanglement entropy $S_A \approx \ell(-\nu \ln(\nu) - (1-\nu) \ln(1-\nu))$ when $\theta \rightarrow \frac{\pi}{2}$ in a linear slice. This is almost independent of dispersion relation.

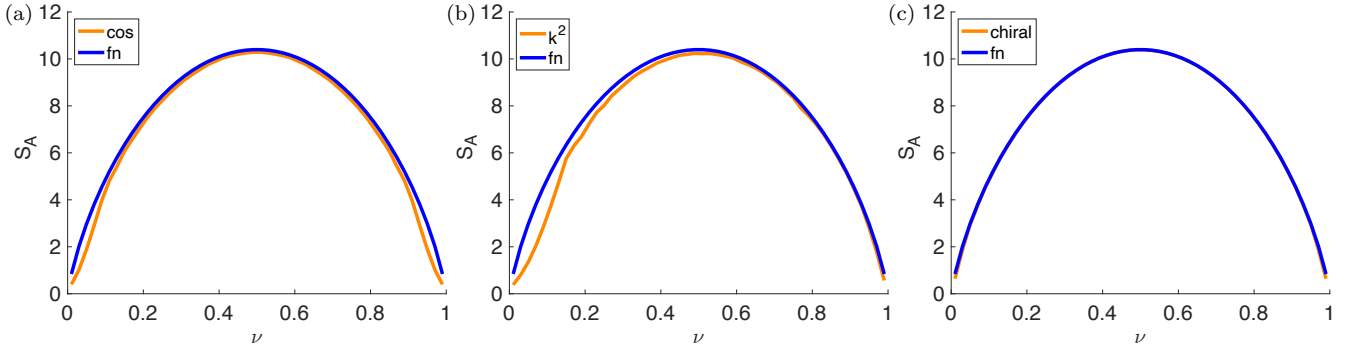


FIG. S8. Zero temperature entanglement entropy S_A versus filling ν in a linear slice with $\ell = 15$ and (a) $t_n E_0 / n = a_0 E_0 \tan(\theta) / v_{\max} = 240$ for cosine dispersion Eq. (S14), (b) $a_0 E_0 \tan(\theta) / v_{\max} = 240$ for quadratic dispersion Eq. (S15), (c) $a_0 E_0 \tan(\theta) / v_{\max} = 150$ for chiral linear dispersion Eq. (S17), where v_{\max} is the maximum Fermi velocity of the corresponding dispersion relation. “fn” stands for the analytic formula $S_A = \ell(-\nu \ln(\nu) - (1-\nu) \ln(1-\nu))$.

VIII. Quantum Mutual Information

When the total Hilbert space decomposes as $h_{\text{tot}} = h_A \otimes h_{A^c}$, the quantum mutual information is

$$\mathcal{I} = S_A + S_{A^c} - S_{\text{tot}} \quad (\text{S18})$$

where S_A (S_{A^c}) is the von Neumann entropy of the reduced density matrix ρ_A (ρ_{A^c}), and S_{tot} is the von Neumann entropy of the state ρ_{tot} .

In order to calculate S_{A^c} , we want to find a orthonormal basis c_B of single fermion annihilation operators that generate h_{A^c} . For the subsystem A we have (Eq. (S8))

$$c = \phi^A a, \quad \phi_{jl}^A = \phi_{l,\mathbf{r}_j} e^{-i\epsilon_l t_j}, \quad 1 \leq j \leq K, \quad 1 \leq l \leq L \quad (\text{S19})$$

If ϕ^A has rank r , suppose

$$c_B = \phi^B a, \quad (\text{S20})$$

where ϕ^B is a complex matrix with dimension $(L-r) \times L$. Because a is the set of single-particle eigenstate annihilation operators, the *rows* of the matrices ϕ^B and ϕ^A together has rank L , the total system size. The rows of ϕ^B can be found by solving for a column vector x of dimension L such that

$$\phi^A x^* = 0 \quad (\text{S21})$$

Numerically, this can be achieved by a QR decomposition of ϕ_A^T :

$$\phi_A^T = QR = [Q_1 \ Q_2] \begin{bmatrix} R_1 \\ 0 \end{bmatrix}, \quad \phi_A = R^T Q^T = R_1^T Q_1^T \quad (\text{S22})$$

where Q is a $L \times L$ unitary matrix, R is a $L \times K$ upper triangular matrix, and R_1 is a $r \times K$ upper triangular matrix. Q_1, Q_2 have dimensions $L \times r, L \times (L-r)$ respectively. By the unitarity of Q ,

$$Q^\dagger Q = I \implies Q_1^\dagger Q_2 = 0 \quad (\text{S23})$$

Define

$$\phi_B = Q_2^T \implies \phi_A \phi_B^\dagger = R_1^T Q_1^T Q_2^* = 0 \quad (\text{S24})$$

so c_B is orthogonal to c . Then we can calculate S_{A^c} by replacing ϕ_A by ϕ_B in Eq. (S8) and the rest of the calculation follows exactly like the calculation of S_A .

IX. Definition of δ Cutoff

To improve numerical precision, we introduce a δ cutoff to the Hilbert space h_A . Suppose the spectrum decomposition of B is

$$B = Q \Lambda Q^\dagger \quad (\text{S25})$$

where Λ is a positive semi-definite diagonal matrix and its diagonal elements are monotonically decreasing: $\Lambda_{nn} \geq \Lambda_{n+1, n+1}$. Because we need to invert Λ to calculate the normalization matrix M , numerical errors on small eigenvalues of Λ will result in large errors on M . To mitigate these errors, we can introduce a cutoff $\delta \geq 0$ to take only the eigenvalues that are bigger than δ . Suppose $\Lambda_{K_\delta, K_\delta}$ is the last eigenvalue that is not smaller than δ

$$\Lambda_{K_\delta, K_\delta} \geq \delta > \Lambda_{K_\delta+1, K_\delta+1} \quad (\text{S26})$$

we can define a $K_\delta \times K_\delta$ matrix

$$\Lambda_\delta \equiv \Lambda_{1:K_\delta, 1:K_\delta} \quad (\text{S27})$$

where $1:n$ stands for indices $\{1, 2, \dots, n\}$ and

$$B \approx Q_\delta \Lambda_\delta Q_\delta^\dagger, \quad Q_\delta \equiv Q_{1:K, 1:K_\delta} \quad (\text{S28})$$

Therefore

$$M = \Lambda_\delta^{-\frac{1}{2}} Q_\delta^\dagger \quad (\text{S29})$$

and everything else follows as in Eq. (S8). In practice, B is never singular unless the number of points K is on the order of L . In this paper, δ is set to 0 unless otherwise mentioned.

X. Total System Size L Dependence

As the total system size L is gradually increased, the zero temperature S_A in the time-direction slice increases from 0 to a stabilizing value, see Fig. S9.

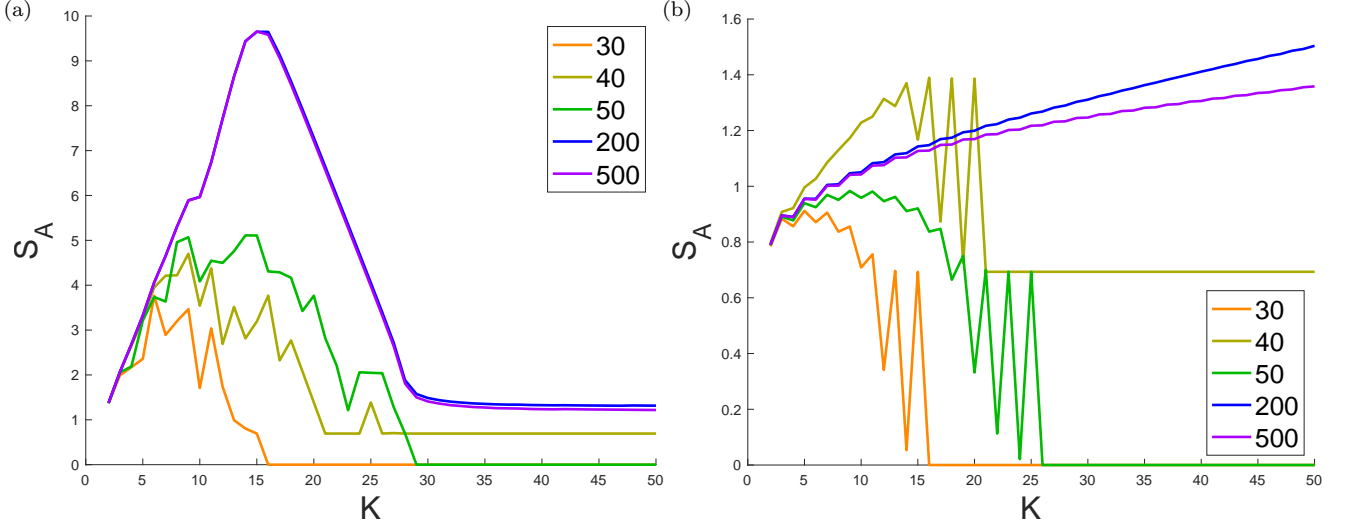


FIG. S9. Zero temperature entanglement entropy S_A of model Eq. (S14) in the time-direction slice with K points for different values of total system size L given in the legend with filling $\nu = \frac{1}{2}$ and $\delta = 10^{-13}$ for (a) fixed $2\pi t/\tau_0 = 168$ and (b) fixing $2\pi t/\tau_0 = 5$.

Now we focus on the $K > L$ regime. For the dispersion relation Eq. (S14) and filling $\nu = 0.5$, $S_A = 0$ when $L/2$ is odd and $S_A = \log(2) = 0.6931$ when $L/2$ is even. This is because of the particular discretization of the spectrum in Eq. (S14), which satisfies $E(k) = E(-k)$. Our spectrum is non-degenerate for the lowest and highest energies, but is doubly degenerate for all energies in between: $-0.5E_0, -0.49E_0, -0.49E_0, \dots, 0.49E_0, 0.49E_0, 0.5E_0$.

Because $\nu = 0.5$, this introduces an even-odd effect with respect to the filling number $L/2$: when $L/2$ is odd, the many-body ground state is a product state $a_{\text{sym}}^\dagger a_{\text{anti}}^\dagger |0\rangle$ of symmetric ($a_{\text{sym}}^\dagger = \frac{1}{\sqrt{2}}(a_k^\dagger + a_{-k}^\dagger)$) and antisymmetric ($a_{\text{anti}}^\dagger = \frac{1}{\sqrt{2}}(a_k^\dagger - a_{-k}^\dagger)$) combinations. When $L/2$ is even, the last pair of a_k, a_{-k} is broken up in the ground state, so we have a superposition $(a_{\text{sym}}^\dagger + a_{\text{anti}}^\dagger)|0\rangle \propto a_k^\dagger|0\rangle$.

As the sub-Hilbert space h_A for the time direction slice at $\mathbf{r}_j = 0$ only contains symmetric combinations ($c_{\mathbf{r}_j}(t_j) = \sum_l a_l \frac{1}{\sqrt{L}} e^{-i\epsilon_l t_j}$), tracing out the antisymmetric part gives $S_A = 0$ when $L/2$ is odd and $S_A = \log(2)$ when $L/2$ is even.

This intuitive picture also implies that S_A drops to 0 or $\log(2)$ around $K = \frac{L}{2}$, because h_A is contained in the symmetric sub-Hilbert space while the symmetric subspace is $2^{\frac{L}{2}}$ dimensional. For more generic dispersion relations and spacetime region A , we expect $S_A = 0$ when $K > L$: because the total Hilbert space h_{tot} is L dimensional while we now have $K > L$ operators to build the sub-Hilbert space h_A , h_A has the potential to be equal to h_{tot} and $S_A = 0$. We also point out that the above analysis is only intuitive: there are special parameters for which S_A is not 0 or $\log(2)$ at $K \gtrsim L/2$.

XI. δ Dependence

In this section we explore the effect of δ defined in Eq. (S27). As shown in Figs. S10a and S10b, when $\delta \approx 1$ the time-direction zero temperature entanglement entropy significantly deviates from the entropy when $\delta = 10^{-14}$. Nonetheless, when $L = 500$, entropy is very robust to changes in δ for all $\delta \leq 0.1$. At large $K > t/\tau_0$, δ has a smoothing effect as shown in Fig. S10a: the curve is very rigged when $\delta = 10^{-15}$ but becomes flat when $\delta \geq 10^{-14}$.

At finite temperature, a large δ flattens out the entropy's linear increase at large $K > t/\tau_0$ (Fig. S10c). This is because S_A is nearly thermal and linear in the number of points K ; a large δ reduces the size of the matrices M and D , so the effective number of points decreases and S_A flattens out. A similar effect is seen for quantum mutual information \mathcal{I} in Fig. S10d: As δ increases, \mathcal{I} at large $K > t/\tau_0$ decreases.

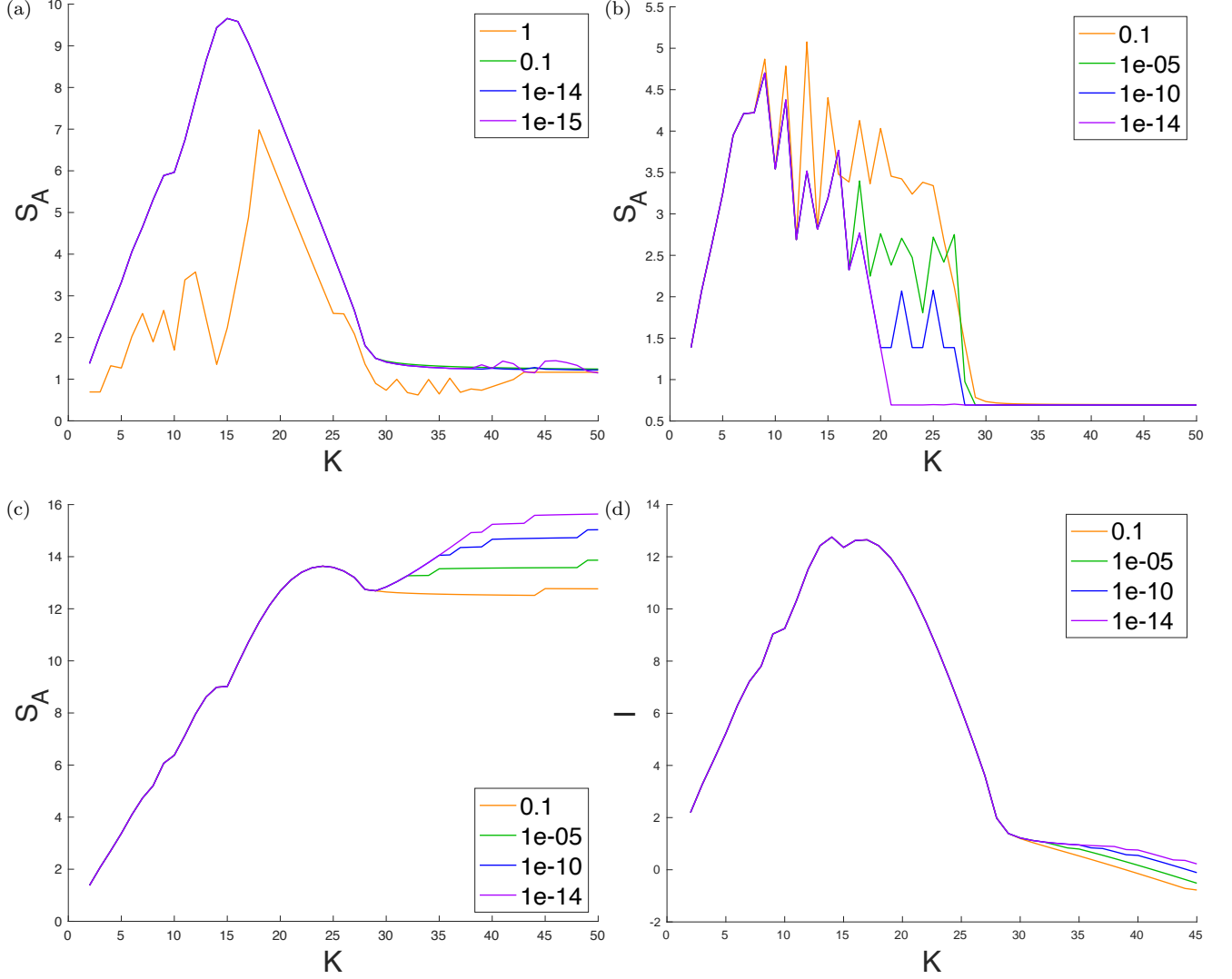


FIG. S10. Entanglement entropy S_A (a-c) and quantum mutual information \mathcal{I} (d) of model Eq. (S14) in the time-direction slice at half-filling $\nu = 0.5$ while fixing $2\pi t/\tau_0 = 168$. Legend is the cutoff δ defined in Eq. (S27), where 1e-n stands for 10^{-n} . (a) $T = 0$ and $L = 500$. (b) $T = 0$ and $L = 40$. (c) $L = 500$, $T/E_0 = 0.15$. (d) $L = 200$ and $T/E_0 = 0.075$.

XII. Slope of Time-direction Entanglement Entropy vs. ν

The fitted ascending slope $(\frac{\partial S_A}{\partial K})_t$ at small K (orange line) for the model in Eq. (S14) is close to $-\nu \ln \nu - (1 - \nu) \ln(1 - \nu)$ (the dashed line). The descending slope (green) is nearly independent of filling ν .

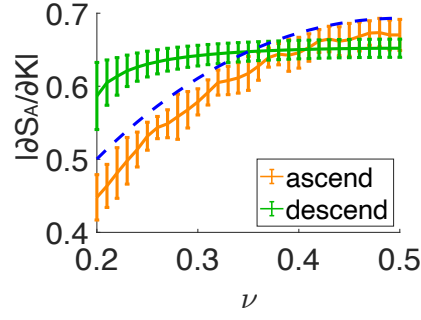


FIG. S11. For the zero temperature entanglement entropy S_A of model Eq. (S14) in the time-direction slice, we plot the absolute value of the slope $\left|\left(\frac{\partial S_A}{\partial K}\right)_t\right|$ with fixed $2\pi t/\tau_0 = 400$ fitted from the ascending region $K \in [2, 6]$ and descending region $K \in [60, 64]$, versus ν (solid lines, error bar 95% confidence). The dashed curve is the function $-\nu \ln(\nu) - (1 - \nu) \ln(1 - \nu)$.

XIII. Non-Eigenstate

Generically, we can consider the non-eigenstate $|\psi\rangle = \prod_{m \in [m_I, m_I + N_f]} c_m^\dagger |0\rangle$ in main text Fig. 3c and 3d. This time we put the time-direction slice at the center of the filling positions with $N_f = 101$ and $m_I = -\frac{N_f - 1}{2}$, in which case $t_L = t_R = 100$. Fig. S12a shows S_A with respect to K at fixed total time t . When $t < t_L$, S_A remains almost zero, while for $t > t_L$, S_A shows a similar curve (with fluctuations) as that of the finite temperature state in main text Fig. 2c. The crossover of S_A as a function of t at $t = t_L$ can be seen more clearly in Fig. S12b, where time spacing τ is fixed.

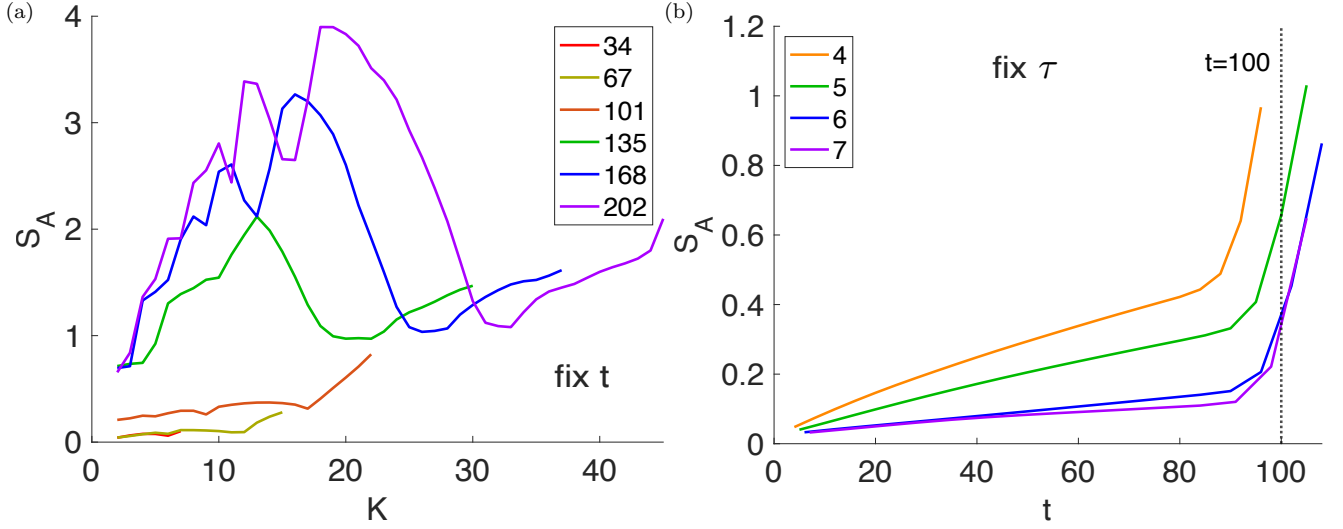


FIG. S12. Entanglement entropy S_A of time-direction slice at site $m = 0$ for non-eigenstates $|\psi\rangle = \prod_{m \in [m_I, m_I + N_f]} c_m^\dagger |0\rangle$ ($L = 1000$), with $N_f = 101$, $m_I = -(N_f - 1)/2$. (a) is calculated with fixed $2\pi t/\tau_0$ given in the legend, while (b) is calculated with fixed $2\pi\tau/\tau_0$ in the legend.